Icarus 200 (2009) 446–462

Contents lists available at ScienceDirect

Icarus

www.elsevier.com/locate/icarus

Geologic context of in situ rocky exposures in Mare Serpentis, Mars: Implications for crust and regolith evolution in the cratered highlands

A.D. Rogers [a,b,*], O. Aharonson [a], J.L. Bandfield [c]

[a] Division of Geological and Planetary Sciences, California Institute of Technology, MC 150-21, Pasadena, CA 91125, United States
[b] Department of Geosciences, Stony Brook University, 255 Earth and Space Sciences, Stony Brook, NY 11794-2100, United States
[c] Department of Earth and Space Sciences, University of Washington, Johnson Hall 070, Box 351310, 4000 15th Avenue NE, Seattle, WA 98195-1310, United States

ARTICLE INFO

Article history:
Received 28 May 2008
Revised 15 October 2008
Accepted 20 November 2008
Available online 16 December 2008

Keywords:
Mars, surface
Infrared observations
Geological processes

ABSTRACT

Global acquisition of infrared spectra and high-resolution visible and infrared imagery has enabled the placement of compositional information within stratigraphic and geologic context. Mare Serpentis, a low albedo region located northwest of Hellas Basin, is rich in spectral and thermophysical diversity and host to numerous isolated exposures of in situ rocky material. Most martian surfaces are dominated by fine-grained particulate materials that bear an uncertain compositional and spatial relationship to their source. Thus location and characterization of in situ rock exposures is important for understanding the origin of highland materials and the processes which have modified those materials. Using spectral, thermophysical and morphologic information, we assess the local and regional stratigraphy of the Mare Serpentis surface in an effort to reconstruct the geologic history of the region. The martian highlands in Mare Serpentis are dominated by two interspersed surface units, which have distinct compositional and thermophysical properties: (1) rock-dominated surfaces relatively enriched in olivine and pyroxene, and depleted in high-silica phases, and (2) sediment or indurated material depleted in olivine and pyroxene, with relatively higher abundance of high-silica phases. This is a major, previously unrecognized trend which appears to be pervasive in the Mare Serpentis region and possibly in other highland areas. The detailed observations have led us to form two hypotheses for the relationship between these two units: either (1) they are related through a widespread mechanical and/or chemical alteration process, where less-mafic plains materials are derived from the mafic bedrock, but have been compositionally altered in the process of regolith formation, or (2) they are stratigraphically distinct units representing separate episodes of upper crust formation. Existing observations suggest that the second scenario is more likely. In this scenario, plains materials represent older, degraded, and possibly altered, "basement" rock, whereas the rocky exposures represent later additions to the crust and are probably volcanic in origin. These hypotheses should be further testable with decimeter-resolution imagery and meter-resolution short wavelength infrared spectra.

1. Introduction

The nature and origin of intercrater surfaces within the martian cratered highlands have been somewhat enigmatic since the Mariner era (Malin, 1976; Greeley and Spudis, 1981; Tanaka et al., 1988; Edgett and Malin, 2002). These surfaces may consist of impact debris, sediments deposited through fluvial and/or aeolian action, and/or volcanic deposits. It is likely that all of these modification processes have played a role in intercrater plains formation to some extent, however the relative contribution of each is largely unknown (Tanaka et al., 1988). Determination of the relative contributions has been hampered by the presence of a veneer of mobile material, ambiguity of or lack of diagnostic morphologic features, and lack of high-resolution geomorphic, thermophysical and compositional data.

The fine component of the martian regolith, here meaning the upper few centimeters of sand and dust deposits found globally across the surface, has been well-characterized with orbiting and landed spectrometers. The composition of dust deposits in high-albedo regions likely includes framework silicate minerals (Bandfield and Smith, 2003; Ruff, 2004), as well as small amounts of carbonates (Bandfield et al., 2003) and nanophase oxides (Allen et al., 1981; Morris et al., 1990; Bell et al., 1993). Low resolution visible/near-infrared (VIS/NIR) and thermal infrared (TIR) remote spectroscopic observations have shown that high- and low-Ca pyroxenes, plagioclase, olivine and high-silica amorphous, primary and/or secondary phase(s) dominate the mineralogy of low-

* Corresponding author at: Department of Geosciences, Stony Brook University, 255 Earth and Space Sciences, Stony Brook, NY 11794-2100, United States. Fax: +1 631 632 1509.
E-mail address: adrogers@notes.cc.sunysb.edu (A.D. Rogers).

0019-1035/$ – see front matter
doi:10.1016/j.icarus.2008.11.026

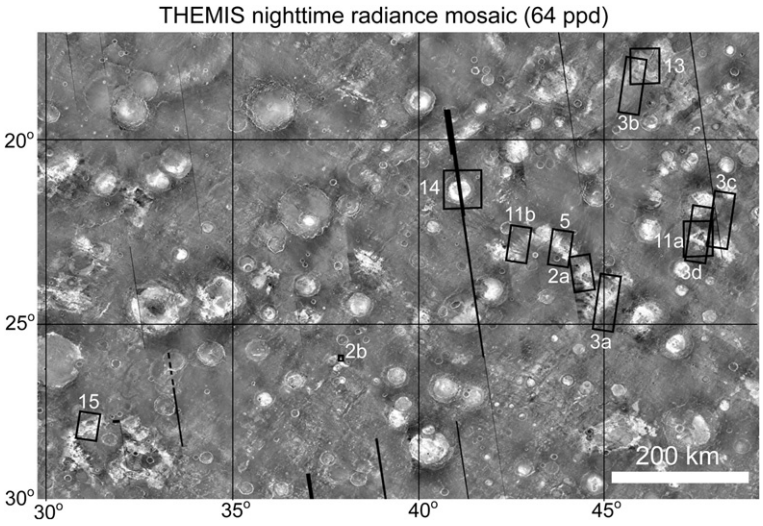

Fig. 1. THEMIS nighttime infrared radiance mosaic of the study region. Outlines of other figure locations are labeled with figure number.

albedo highland regions (see reviews and summaries by Singer et al., 1979; Soderblom, 1992; Roush et al., 1993; Christensen et al., 2001; Bandfield, 2002; Bibring et al., 2005; Christensen et al., 2005; Ruff et al., 2006; Farrand et al., 2007; Rogers and Christensen, 2007; Farrand et al., 2008; Rogers and Aharonson, 2008). The southern highlands show some regional variability, with the most dominant composition consisting primarily of low- and high-Ca pyroxenes, plagioclase, high-silica phases and olivine (Mustard et al., 2005; Rogers and Christensen, 2007). Local-scale enrichments of olivine, high-silica phases, high-Ca clinopyroxene, low-Ca pyroxene, quartz/feldspars, sulfate, phyllosilicate and gray crystalline hematite have been identified in the highlands with Mars Global Surveyor Thermal Emission Spectrometer (TES), Mars Odyssey Thermal Emission Imaging System (THEMIS), Mars Express Observatoire pour la Minéralogie, l'Eau, les Glaces, et l'Activité (OMEGA), and Mars Reconnaissance Orbiter (MRO) Compact Reconnaissance Imaging Spectrometer for Mars (CRISM) data sets (Christensen et al., 2000a, 2003; Hamilton et al., 2003; Hoefen et al., 2003; Bandfield et al., 2004a; Hamilton, 2004; Bibring et al., 2005; Christensen et al., 2005; Gendrin et al., 2005; Hamilton and Christensen, 2005; Mustard et al., 2005; Poulet et al., 2005; Rogers et al., 2005; Bandfield, 2006; Glotch and Rogers, 2007; Murchie et al., 2007), however systematic mapping of these phases at high-resolution has not yet been carried out.

High resolution thermophysical and spectroscopic data sets permit examination of the geology of highland materials in detail. In particular, it is now possible to identify and resolve exposures of bedrock and other locally-derived rocky material such as boulders, cobbles and pebbles, using thermophysical observations (Christensen et al., 2003; Rogers et al., 2005; Fergason et al., 2006; Edwards et al., 2005). Most martian surfaces are dominated by fine-grained particulate materials that bear an uncertain compositional and spatial relationship to their source. Location and characterization of in situ rocky exposures is important for understanding the origin of highland materials and the processes which have modified those materials.

In an effort to contribute to current understanding of highland origin, stratigraphy and evolution, this study focuses on the characterization of rock exposures and surrounding materials in a typical region of the cratered highlands, Mare Serpentis. Mare Serpentis is a low-albedo region between 30–50° E and 15–30° S, northwest of Hellas Basin (Fig. 1). This region was chosen because it contains a concentration of several intercrater plain rocky exposures within a relatively small area (Edwards et al., 2005). In addition, the location within a low-albedo area facilitates spectroscopic characterization due to the relative lack of dust cover. The goals of this study are to: (1) understand how the well-characterized regolith fine component relates to in-place rock, (2) determine the degree of vertical and lateral compositional heterogeneity within exposed rocky surfaces, and (3) determine the geologic origin of in situ material in Mare Serpentis.

2. Methods

Thermal inertia (TI) values derived from THEMIS (Christensen et al., 2004) surface temperature data using the method of Fergason et al. (2006) are used to locate rock-dominated surfaces. All available THEMIS images were initially searched for surfaces with TI values of 1200 (units of $J\,m^{-2}\,K^{-1}\,s^{-1/2}$ are used throughout this manuscript and are hereafter omitted) or higher. This value was chosen as a conservative threshold for identifying locally-derived material. With the exception of outflow channel flood deposits, crater ejecta and rocks derived from nearby cliffs, this TI value ensures that the infrared spectral signature is dominated by directly-derived boulders, cobbles and pebbles, rather than potentially regionally-homogenized sand, silt, and dust (Fergason et al., 2006). In Mare Serpentis, surfaces with TI values of 1200 are typically restricted to areas of only a few spatially contiguous THEMIS pixels. However, the geomorphic properties associated with a TI value of 1200 in Mare Serpentis (a pitted, resistant texture in Mars Orbiter Camera (MOC) imagery) typically extends well beyond these small areas, to include surfaces with TI values as low as ~500 (Fig. 2). Though lower than 1200, TI values >500 are high relative to the majority of the martian surface (e.g., Putzig et al., 2005) and are consistent with clast sizes greater than or equal to coarse gravel (Presley and Christensen, 1997). For relatively flat plains surfaces, coarse gravel is not likely to have been transported far from its original source, thus the TI value associated with in situ rock exposures in this study was relaxed to a minimum of 500. In summary, rock exposures in Mare Serpentis are distinguished by having TI values greater than 500 and by a characteristic texture in high-resolution images (Fig. 2). The majority of these exposures contain some THEMIS pixels with TI values greater than 900, whereas four of them contain values of 1200 or more.

Portions of THEMIS daytime infrared images with average surface temperatures >245 K (Bandfield et al., 2004b), TES albedo values <0.16, and TES 1350–1400 cm^{-1} emissivity >0.960 (Ruff and Christensen, 2002) were selected for detailed spectral analysis of the rocky exposures and surrounding materials. These restrictions ensured high signal to noise ratio data of surfaces free of ob-

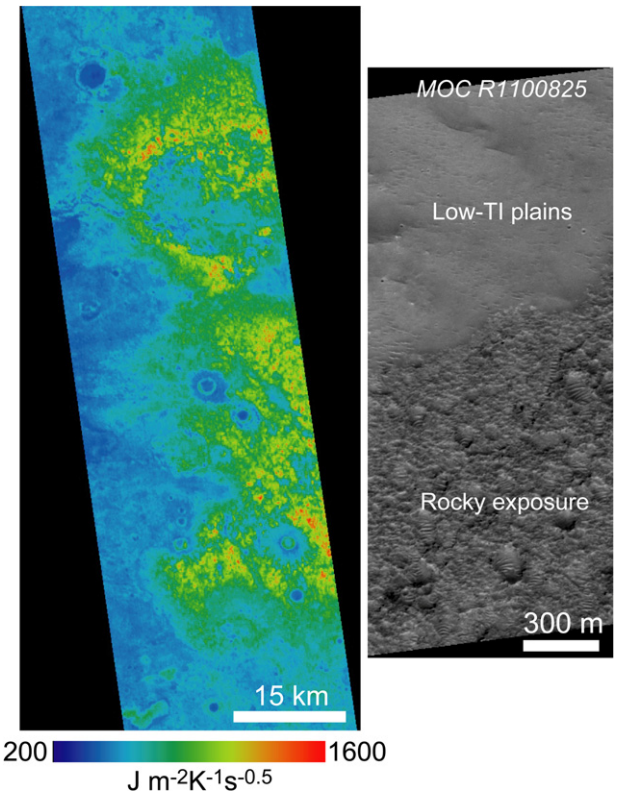

Fig. 2. (a) THEMIS TI derived from night time image I17841010 of a typical rocky exposure and surroundings. Values greater than 500 (green to red) indicate rocky material, whereas blue coloration indicates lower TI plains. (b) MOC image R11/00825 showing typical morphology of high TI rocky material and low TI plains. See Fig. 1 for context. (For interpretation of the references to color in this figure legend, the reader is referred to the web version of this article.)

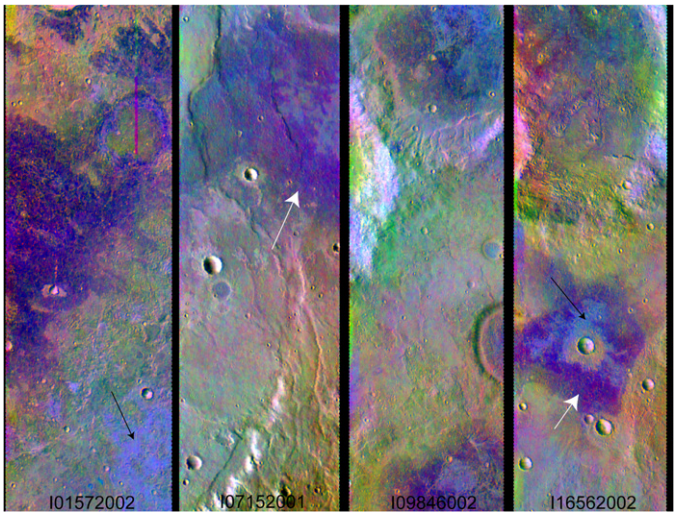

Fig. 3. THEMIS daytime radiance images, decorrelation stretched using bands 8/7/5 as red, green and blue. Each panel is ~30 km wide. Rocky exposures appear magenta (white arrows point to typical examples), while surrounding low TI plains appear greenish-yellow or pink. Light blue units (black arrows point to examples) are found associated with rocky surfaces and plains. See Fig. 1 for context.

scuring dust cover. The images were corrected for time-dependent detector temperature changes and the constant atmospheric radiance component using the methods of Bandfield et al. (2004b), and converted to apparent emissivity using the emissivity normalization method (Gillespie, 1985; Christensen, 1998). Emissivity images were examined for spectral variability using a decorrelation stretch (DCS, Gillespie et al., 1986) of three different spectral band combinations (8/7/5, 9/6/4, and 6/4/2, corresponding with 11.8/11.0/9.4 μm, 12.6/10.2/8.6 μm, and 10.2/8.6/6.8 μm, respectively).

TES spectra that cover and isolate spectrally-uniform areas within the study area (identified using the THEMIS DCS images) were selected for derivation of surface emissivity and mineral abundance estimation. Only TES emissivity spectra associated with surface temperatures >270 K, dust extinctions <0.15 and ice extinctions <0.04 were used. The selected spectra are averaged and the atmospheric components are removed using the deconvolution method of Smith et al. (2000). This method uses a spectral library of potential surface endmembers, atmospheric endmembers (Bandfield et al., 2000a; Bandfield, 2002), and blackbody to obtain a linear least-squares fit to the measured TES effective emissivity spectrum. The atmospheric component spectra are scaled according to their modeled concentrations and subtracted from the measured spectrum to produce the surface emissivity spectrum. This process is conducted for as many spectra as possible that cover the region of interest, preferably from varying atmospheric conditions, to build confidence in the derived surface emissivity spectrum. To derive mineral abundance estimates from TES spectra, the average surface emissivity spectrum is modeled using a best-fit linear combination (e.g., the algorithm of Ramsey and Christensen, 1998; revised according to Rogers and Aharonson, 2008) of emission spectra of minerals (Christensen et al., 2000b), mineraloids, glasses, and martian surface dust (Bandfield and Smith, 2003). The library constructed for this study is similar to that of Rogers and Christensen (2007), but with additional sulfate and phyllosilicate mineral spectra. To compensate for the increase in library size, a few spectra from slightly overrepresented mineral groups (alkali feldspar, plagioclase, serpentine and amphibole) in the Rogers and Christensen (2007) library were removed.

OMEGA data are also used to examine the mineralogic composition of bedrock and surrounding surfaces. Only data from the OMEGA C-channel (0.9–2.7 μm) are used, due to current complications associated with interpreting the *L*-channel data (2.5–5.1 μm) (e.g., Mustard et al., 2007). To ensure retrieval of the highest-quality spectra, data associated with incidence angles >70° and emergence angles >20° were excluded (Pelkey et al., 2007). The data are calibrated and converted to reflectance using the methods outlined in the OMEGA data set tutorial available from the Mars Express archive (http://www.rssd.esa.int/index.php?project=PSA&page=MarsExpress). The data are corrected for atmospheric contributions using the method of Bibring et al. (2005). Mineral indicator maps are produced from OMEGA data using the spectral indices identified by Pelkey et al. (2007). Mineral detections suggested by these maps are verified by visual inspection of spectra from each detection and comparison with laboratory spectra of minerals available from the NASA RELAB facility at Brown University. Instrumental artifacts such as "hot" and "dead" channels and perturbed pixels as well as atmospheric features such as water ice clouds are avoided using the methods described in the OMEGA software reduction document (from the Mars Express Archive) and in Pelkey et al. (2007).

High resolution MOC narrow angle (~1.5–3.0 m/pixel) and THEMIS visible images (~18 m/pixel) are used to characterize fine scale surface textures and geomorphology. Topographic profiles extracted from MOLA elevation data binned at 128 ppd (Smith et al., 2001) are used to measure thicknesses and elevations of units. TES albedo, MOC wide angle, MOC narrow angle, and THEMIS VIS images are used to examine relative brightness variations within the study region. At the time of writing, MRO CRISM, Context Camera (CTX), and High Resolution Imaging Science Experiment (HiRISE) data over the rocky exposures are not publicly available.

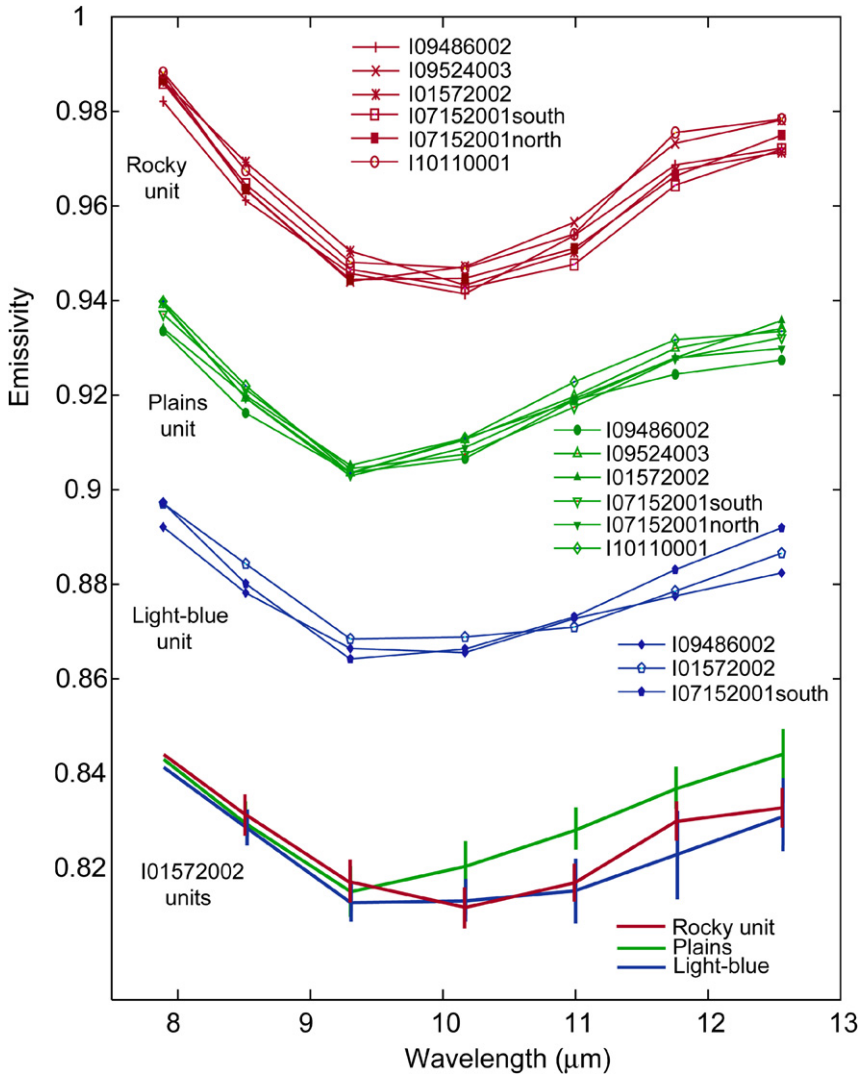

Fig. 4. Atmospherically-corrected THEMIS spectra extracted from rocky outcrops, plains, and light-blue spectral units. The upper three sets of spectra show the typical spectral character of the three units, extracted from multiple images. The lower set of spectra are from a single THEMIS image, showing the typical variance observed on the spectral averages. The spectra from DCS light blue materials are not usually statistically separable from those of the rocky surfaces, despite their distinct distributions. (For interpretation of the references to color in this figure legend, the reader is referred to the web version of this article.)

3. Results

3.1. Thermal inertia

The TI values of rocky exposures are typically between 500–1600 (Section 2). Fig. 2 shows typical spatial variability in TI within a rocky exposure. Where crater ejecta blankets are distinguishable in either nighttime IR or visible data, the TI of the ejecta blankets typically ranges between 160–270. Plains materials that are not obviously part of impact ejecta blankets exhibit TI values between 120–420.

3.2. Composition

THEMIS DCS images reveal that the in situ rock exposures are spectrally distinct from surrounding materials (Fig. 3). The exposures appear magenta in band 8-7-5 DCS images, while lower TI surrounding materials (hereafter also referred to as "lower TI plains") appear greenish-yellow or pink. Representative THEMIS spectra from the rock exposures are compared with surrounding plains surfaces (Fig. 4). The spectral differences, mainly a lower emissivity in bands 6 (10.2 μm) and 7 (11.0 μm), are consistent with the rock exposures containing a higher abundance of pyroxene and/or olivine than the surrounding plains. Crater ejecta materials are spectrally indistinguishable from the surrounding plains (Fig. 3). Also commonly observed in the region are small isolated units that appear light blue in 8/7/5 stretches (Figs. 3–4). The DCS light blue units are similar in spectral shape to the lower TI plains, but have a negative slope imposed on the overall spectral shape. The light blue units are also associated with a lower TI than the rocky exposures, with values of 160–440.

Though the rock exposures typically appear spectrally homogeneous in DCS 8/7/5 images, there are exceptions observed in some areas, particularly in the warmest images available (bedrock surface temperatures >240 K). In these images, the exposures exhibit small interspersed areas of red and blue spectral units (in 8/7/5 band combinations, Fig. 5). The DCS red unit exhibits a distinctly lower emissivity in Band 4 (8.6 μm) and higher emissivity in Bands 6–8 (10.2–11.8 μm), relative to the DCS blue unit. The spectral variations also correspond with differences in albedo and TI. The DCS red regions have a relatively higher albedo and exhibit the highest TI within the exposure, while the DCS blue regions are darker and have a slightly lower TI. The spectral differences sometimes observed within the exposures are too small to be discernable in

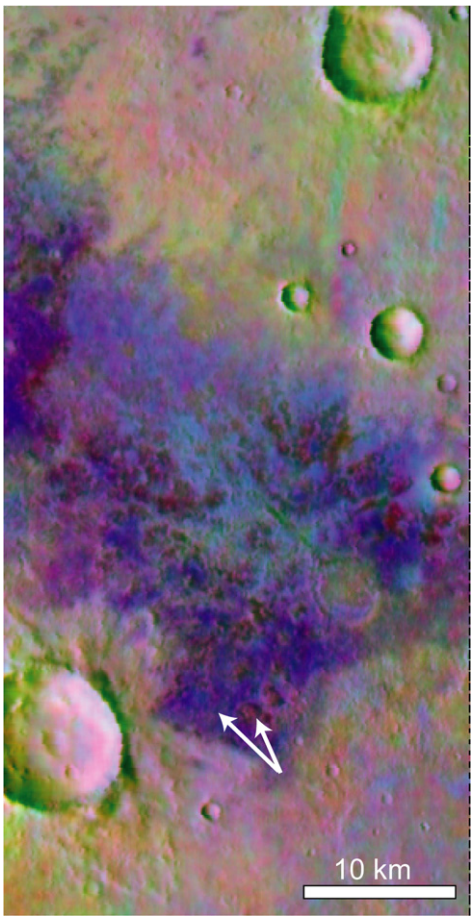

Fig. 5. Portion of THEMIS daytime radiance image I08675002, decorrelation stretched using bands 8/7/5 as red–green–blue. Arrows point to small scale spatial heterogeneity in composition that is occasionally observed within the rocky exposures. See Fig. 1 for context. (For interpretation of the references to color in this figure legend, the reader is referred to the web version of this article.)

TES or OMEGA data. However the differences are consistent with the DCS red unit having increased sulfate and/or high silica phases, or with simply being less mafic than the bluer regions.

The DCS light-blue units found within the region are also too small for detailed compositional analysis with existing data that meet our selection constraints, however the spectral character and mineralogic composition of rocky exposures and surrounding low TI plains were determined using TES and OMEGA observations (Figs. 6 and 7). The spectral difference between the rocky materials and surrounding plains is similar in character, but not as extreme in TES spectra as that observed in THEMIS spectra (Fig. 6). This may be attributed to the difference in spatial resolution between the THEMIS and TES instruments. Small areas with the strongest DCS magenta colors were selected for the THEMIS spectral averages in Fig. 4. Larger regions, such as at the km scale of TES observations, incorporate some of the plains materials within the measurements.

Fig. 6 shows the TES-derived surface emissivity for rock and surrounding lower-TI plains derived from five orbits. The most significant difference between the spectral shapes of the two units is found in the region between ~400 and 500 cm^{-1}. In this region, the rock exposures exhibit a broad emissivity peak whereas it is narrower and shifted towards longer wavelengths in lower-TI surfaces. Rock exposures also exhibit a positive slope in emissivity between 507 and 444 cm^{-1}, while surrounding lower-TI materials exhibit a negative emissivity slope in this region. These long-wavelength differences are attributable to variations in olivine, pyroxene, and high-silica phase abundances. Crater ejecta blankets have mineral abundances that are similar to the plains, and are spectrally indistinguishable from the plains.

Table 1
Spectral library.[a]

	Quartz BUR-4120	Quartz
	Microcline BUR-3460	Alkali feldspar
	Albite WAR-0235	Plagioclase
	Oligoclase BUR-060D	
	Andesine WAR-0024	
	Labradorite BUR-3080A	
	Bytownite WAR-1384	
	Anorthite BUR-340	
	Bronzite NMNH-93527	Orthopyroxene
	Enstatite HS-9.4B	
	Hypersthene NMNH-B18247	
(1)	Avg. Lindsley pigeonite	Low-Ca clinopyroxene
	Diopside WAR-6474	High-Ca clinopyroxene
	Augite NMNH-9780	
	Augite NMHN-122302	
	Hedenbergite manganoan DSM-HED01	
	Forsterite BUR-3720A	Olivine
	Fayalite WAR-RGFAY01	
(2)	KI 3362 Fo60	
(2)	KI 3115 Fo68	
(2)	KI 3373 Fo35	
(2)	KI 3008 Fo10	
	Biotite BUR-840	Phyllosilicates
	Muscovite WAR-5474	
	Serpentine HS-8.4B	
(3)	Illite Imt-1 <0.2 μm (pellet)	
	Ca-montmorillonite solid STx-1	
(4)	Saponite (Eb-1?) <0.2 μm (pellet)	
(3)	SWy-1 <0.2 μm (pellet)	
(5)	K-rich Glass	Amorphous silica
(5)	SiO_2 Glass	
(6)	Opal-A (01-011)	
(7)	Al-opal	
	Magnesiohastingsite HS-115.4B	Amphibole
	Magnesiohornblende WAR-0354	
(8)	Ave. Meridiani and Aram Hematite (TT derived)	Oxide
	Anhydrite ML-S9	Sulfate
	Gypsum ML-S6	
(9)	Kieserite	
	Calcite C40	Carbonate
	Dolomite C20	
(10)	Crystalline heulandite	Zeolite
(10)	Crystalline stilbite	

[a] Mineral spectra are from the ASU spectral library available online at http://tes.asu.edu (Christensen et al., 2000b), with the following exceptions: (1) Wyatt et al. (2001); (2) provided by V.E. Hamilton; (3) Michalski et al. (2006); (4) Michalski et al. (2005); (5) Wyatt et al. (2001); (6) Michalski et al. (2003); (7) provided by M.D. Kraft; (8) Glotch et al. (2004); (9) provided by A.M. Baldridge; (10) spectra described in Ruff (2004).

TES spectra from two orbits with the most distinct difference in spectral shape between the low-TI plains and rock exposures were selected for linear least squares minimization modeling using the library in Table 1 (Fig. 6b). Because the TES spectra do not completely isolate the rocky exposures from plains materials, the TES-derived feldspar, pyroxene, olivine and high-silica phase abundances of the rocky exposures do not differ from plains materials outside of the stated uncertainties (Table 2). However, derived mineral abundances from individual orbits may be used to identify trends in compositional difference between the rocky exposures and plains. In general, high inertia units have more py-

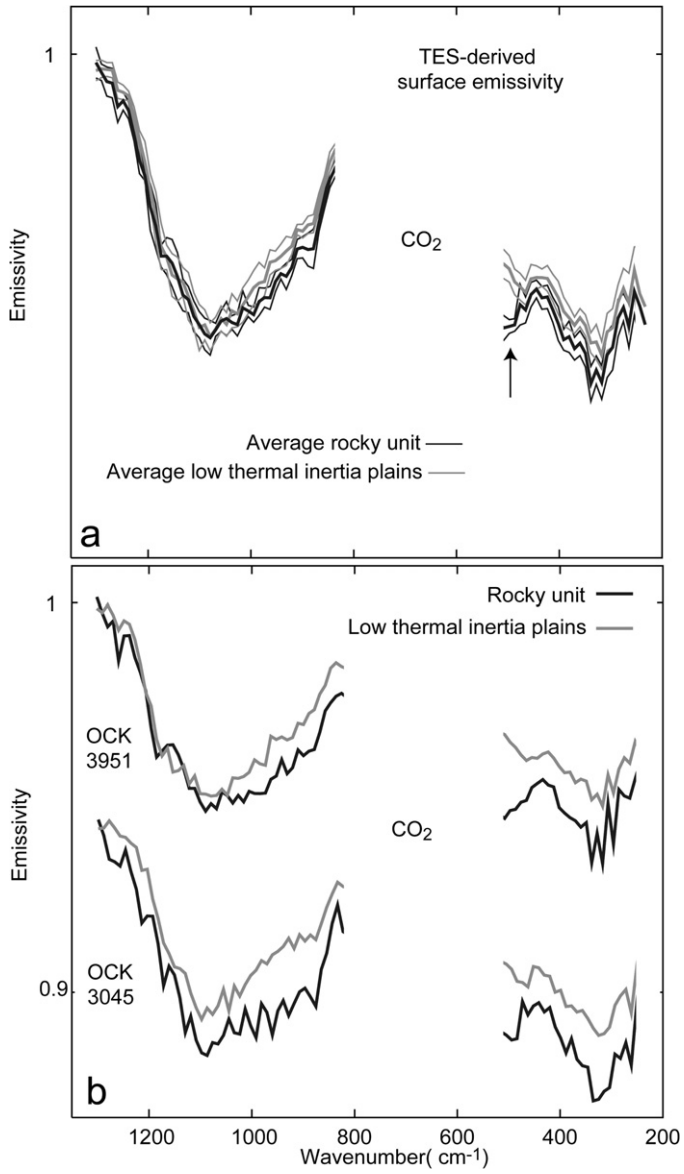

Fig. 6. (a) Average surface emissivity from rocky exposures and surrounding plains, derived from five TES orbits. The variance on each average is shown in the same line color. Arrow points to spectral region that most distinguishes the two units. (b) TES derived surface emissivity from rocky surfaces and low TI plains, for two orbits. The differences between the two units are more apparent in these orbits.

roxene and olivine, and less high-silica phases, than surrounding plains (Table 2). This mineralogic trend is consistent with the distinct spectral character of the two units observed with THEMIS data (Fig. 4). In the ~8–12 μm spectral region, the position of the silicate absorption shifts to longer wavelengths with increasingly mafic composition (e.g., Lyon, 1965). Thus the THEMIS-derived surface emissivity analysis (Fig. 4) is a semi-independent method that supports the mineralogic trends identified from TES data (Table 2). Furthermore, the differences in TES and THEMIS spectra between the rocky exposures and plains are similar to those between the two global spectral units observed in TES data, Surface Types 1 and 2 (Bandfield et al., 2000b), respectively. The mineralogic differences between those two surface types may be summarized as higher pyroxene abundance and lower feldspar and high-silica phase abundance in Surface Type 1, further supporting the interpreted mineralogy of the rock and plains units.

There is a possibility that the observed variations in plagioclase/pyroxene ratios are due to a spectral effect caused by non-linear mixing. Preliminary work by Rampe et al. (2007) shows that laboratory spectra of particulate mixtures with minor amounts of alteration products are subject to non-linear mixing. For example, they find that addition of <5% amorphous silica to a mixture of equal portions of augite and labradorite causes apparent increases in plagioclase/pyroxene ratios derived from spectral unmixing. If this process is occurring in Mare Serpentis, it would imply that the lower-TI surfaces are actually similar in plagioclase/pyroxene ratio to the rocky surfaces, but simply contain a higher abundance of high-silica phases. While this process may be partially contributing to the observed compositional trends, it is likely not the dominant factor. In the preliminary work of Rampe et al. (2007), the silica added to the mixtures was not commonly detected in spectral models, even with known abundances of up to 30%. Here, the TES modeling shows a difference in silica, suggesting that all phases are being identified in proper proportions. In addition, it is geologically unlikely that a difference in high-silica phases, but no other phases, would occur preferentially in plains materials, but not in adjacent rocky surfaces.

Only one OMEGA image of sufficient quality and spatial resolution that covers both rocky materials and surrounding surfaces was publicly available at the time of analysis. There may be subtle differences in pyroxene composition between the two units. Fig. 7 shows spectra extracted from each of the surfaces. The spectral shapes are consistent with the presence of both low- and high-Ca pyroxenes; however, the undifferentiated plains spectrum does have a slightly broader peak at 1.5 μm, and less of an overall negative slope, suggesting it may contain a higher abundance of high-Ca pyroxene than the rocky exposures. However, the spectral differences could also be due to a spectral slope effect rather than to composition. As with the TES data, the differences between OMEGA spectral averages from each unit are likely to be somewhat affected by limited spatial resolution compared to the THEMIS data. Mineral parameter maps derived from the OMEGA data do not show any detectable olivine in either the rocky exposures or surrounding plains. The difficulty in detecting olivine in pyroxene-rich surfaces measured by OMEGA data has been noted for the Meridiani Planum region (Arvidson et al., 2006). In that study, Arvidson et al., suggest that one reason for this may be increased backscattering of pyroxene crystals relative to olivine. Alternatively, nanophase metallic iron particles finely dispersed within the olivine could also obscure detection in the VIS/NIR spectral region (Pieters et al., 2008).

3.3. Morphology, texture and relative albedo

Fig. 8 shows two MOC images that cover the spectral units identified in THEMIS data. Rocky materials exhibit a consistent morphology in MOC imagery (Figs. 2b, 8a and 8b), and commonly appear pitted and rough compared to the surrounding plains (Fig. 2b). Small dark-toned bedforms are sometimes observed within the pits. Brightness variations are commonly observed within the rocky exposures (Fig. 8). These appear to be due to actual differences in rock tone, rather than variations in amount of sediment cover, because bedforms are not regularly observed in the darker toned areas. However, it is possible that sand could be concentrated in small crevasses in the bedrock, which could give the appearance of a darker tone. THEMIS TI values of the darker toned areas are slightly lower than the bright toned areas, consistent with increased dark sand cover.

Low-TI plains and crater ejecta blankets have a degraded appearance in MOC imagery relative to the rock exposures. The plains do not have a consistent morphology; a range of features including bedforms, dark toned sand sheets, secondary craters, ridges, mesas and rough/pitted material are commonly observed (Figs. 8 and 9). Crater ejecta blankets and low-TI plains are not consistently lighter

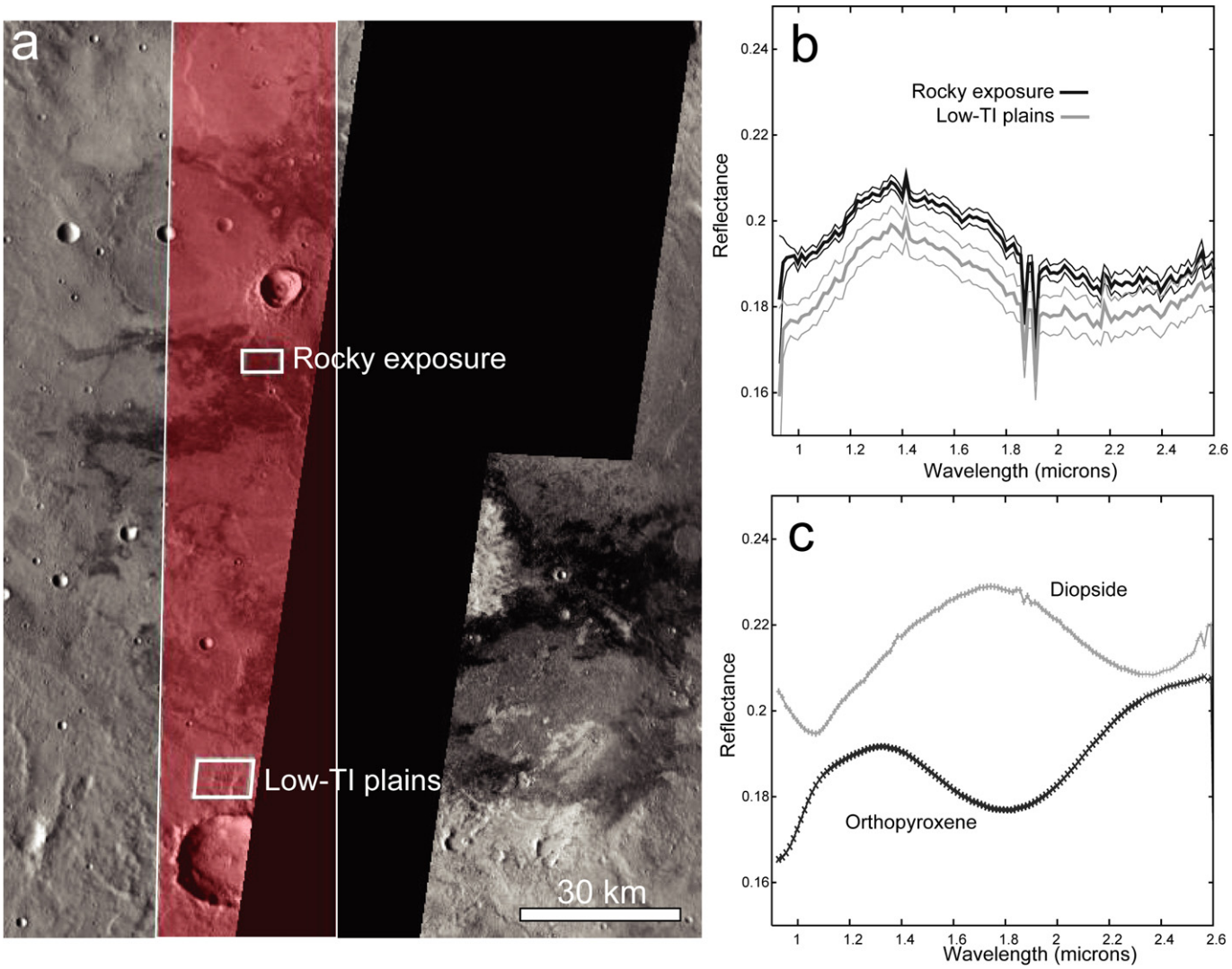

Fig. 7. (a) THEMIS daytime radiance mosaic of rocky exposures and surrounding plains. The red polygon indicates the area of OMEGA image 1157_01. White boxes show regions where OMEGA spectra were extracted for comparison. (b) Atmospherically corrected OMEGA spectra from regions shown in (a). Thick lines are the average spectrum and thinner lines represent one standard deviation. (c) Laboratory spectra of diopside and orthopyroxene, provided by the NASA RELAB facility at Brown University.

Table 2
TES-derived mineral abundances.

	OCK 3951		OCK 3045	
	Rocky unit	Plains	Rocky unit	Plains
Quartz	1 ± 2	2 ± 1	1 ± 2	0 ± 0
Feldspar	32 ± 9	37 ± 6	25 ± 10	28 ± 7
Pyroxene	27 ± 10	18 ± 4	37 ± 13	27 ± 8
Olivine	4 ± 5	6 ± 2	10 ± 4	1 ± 3
High-silica	13 ± 7	21 ± 5	11 ± 9	23 ± 5
Amphibole	5 ± 5	0 ± 0	0 ± 0	0 ± 0
Hematite	4 ± 4	3 ± 2	3 ± 4	2 ± 3
Sulfate	10 ± 4	10 ± 4	7 ± 4	11 ± 3
Carbonate	4 ± 2	3 ± 1	6 ± 1	8 ± 1
Plag/pyx	1.2 ± 0.7	2.1 ± 0.9	0.7 ± 0.5	1.1 ± 0.6

or darker toned than high-TI rocky surfaces. This likely reflects regional variations in dust or sediment cover. TES albedo values of the region range from 0.11 to 0.16, also indicating variable minor contributions of dust.

The light blue spectral unit is commonly lighter toned than the rock exposures or low-TI plains it overlies (Figs. 8a and 10), and therefore the light blue spectral unit is hereafter referred to as the "light-toned" unit. Light toned bedforms are commonly observed on top of the light toned coherent material (Figs. 8a and 10).

3.4. Geologic context of in situ rock exposures

Rock exposures occur in intercrater plains and crater floors. They commonly overlie, but also are regularly superposed by, ejecta blankets from large diameter (>40 km) craters (Figs. 1 and 11). This suggests that the rock exposures, if they represent a single stratigraphic unit, were emplaced during the same time period that these large craters formed (late Noachian/early Hesperian) (Greeley and Guest, 1987). The rock exposures occur at a range of elevations (650–2750 m) and are sometimes deformed by wrinkle ridges. Rocky materials with compositions similar to these may have a wider distribution outside the study region, indicated by preliminary examination of THEMIS DCS images and THEMIS and TES surface emissivity spectra in other cratered highland regions.

The margins of the rock exposures are sharp, with a distinct change in morphology from rocky-type to low-TI plains-type within a distance of 5–10 m. The nature of the contact between the rocky materials and low-TI plains is not evident from available imagery or topographic information. High-resolution images were examined for lobate margins or scarps, which might indicate the stratigraphic position relative to the plains, however no diagnostic examples were found. The contacts between the rocky surface margins and adjacent plains are sharp relative to the spatial reso-

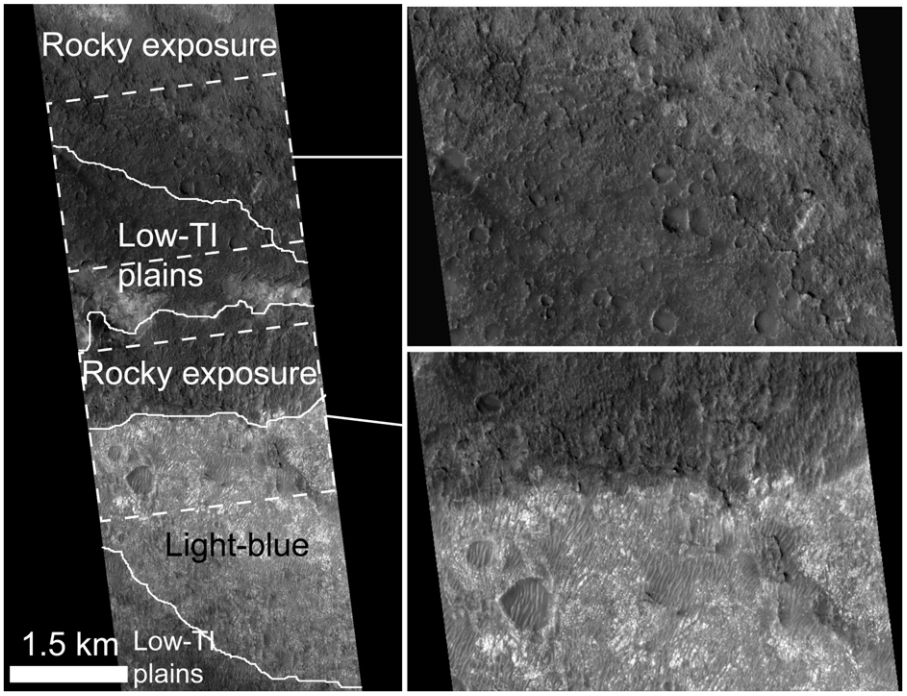

(a)

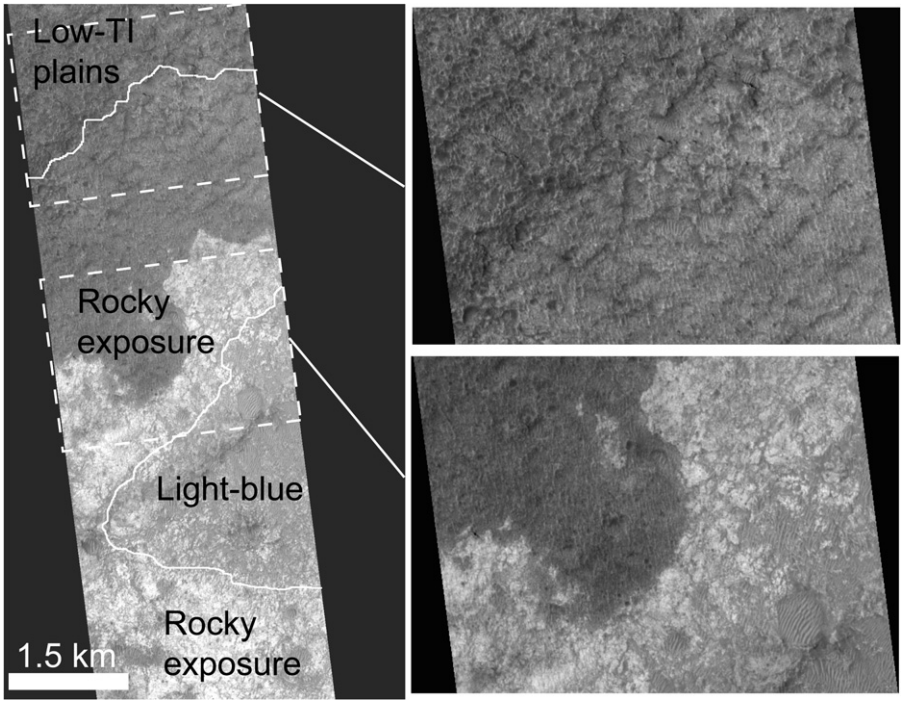

(b)

Fig. 8. (a) MOC image R1101489 of rock outcrop, DCS light-blue surface and plains textures and tone. All three units are variable in tone. (b) MOC image E1004226 of rock outcrop, DCS light-blue surface and plains unit textures and tone. All three units are variable in tone.

lution of individual orbit track MOLA topographic profiles, and thus the fine topographic relief across the margins cannot be resolved. Because of this, altimetric data also do not provide a unique stratigraphic relationship.

4. Discussion

4.1. Geologic units

On the basis of TI, spectral properties and geomorphology, four units are distinguished in the study region (Table 3). A geologic sketch map illustrating the typical spatial relationships in the region is shown in Fig. 12. A rocky unit, characterized by high TI (>500), an olivine- and pyroxene-rich mineralogical composition, and an erosion-resistant morphology, is found in intercrater plains as well on the floors of craters. Crater ejecta materials are observed either in visible or nighttime infrared imagery. Plains that are generally undifferentiated with respect to composition, morphology, and TI comprise the third unit. The undifferentiated plains and crater ejecta units are compositionally distinct from the rocky unit, consisting of less pyroxene and/or olivine (and therefore higher

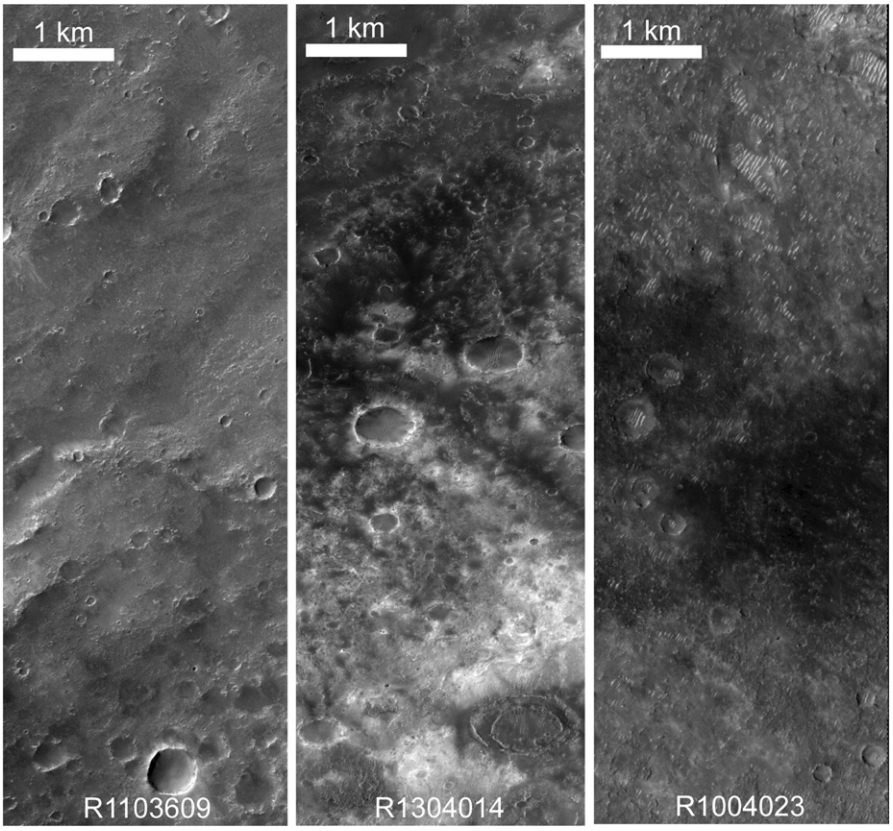

Fig. 9. Three MOC images showing range of morphologies observed on low-TI plains.

plagioclase/pyroxene ratios), and more high-silica phases. A light-toned unit is distinguished by its spectral character, relatively high albedo, and low TI. THEMIS spectra over the light toned unit are consistent with undifferentiated plains materials with contributions of minor amounts of dust. The Mars Reconnaissance Orbiter CRISM instrument, with a spatial resolution of ~38 m or better, may reveal more information about variability within the rocky exposures, as well as the detailed mineralogical composition of the light-toned unit.

4.2. Stratigraphic relationships

With the exception of the rocky unit, the geologic units defined above exhibit TI values of 120 to 440, consistent with either unconsolidated fine sediment to fine gravel (100 to ~3000 μm) or weakly to moderately indurated material. With the possibility that the undifferentiated plains are unconsolidated sediment, it is difficult to assess the stratigraphic relationship between the plains and rocky units. However, for the sake of revealing possible geologic relationships, we temporarily assume that the undifferentiated plains are an indurated unit and try to assess its stratigraphic position relative to the rocky unit.

Morphology and topography of the outcrop edges do not reveal whether they are depositional margins or erosional boundaries (Section 3.4), however there are other observations that can be used to assess stratigraphic position. Crater rims, walls and ejecta are spectrally identical to the undifferentiated plains (Section 3.2), suggesting that they are part of the same unit. The rocky unit is commonly found abutting crater rims, and covering crater floors, indicating that it was deposited after these craters formed (Fig. 11a). Thus the observation that the rocky unit appears to have formed after the craters suggests that it also formed after the undifferentiated plains. In addition, ejecta blankets from craters with diameters larger than ~3 km usually exhibit plains-like spectral properties (Figs. 11a and 11b), regardless of whether the impact sites are on the undifferentiated plains or on the bedrock. This observation suggests that impacts greater than ~3 km diameter have excavated plains-like material from underneath the rocky unit, and that relative to the plains, the rock exposures are volumetrically minor contributions to the surface. It is possible that materials with the plains-like composition could be derived from the bedrock through the impact process itself (e.g., Hörz et al., 1984) (Section 4.3). However, there is at least one example of a ~3 km crater within the rocky unit that is spectrally identical to that unit (Fig. 13), rather than to the undifferentiated plains. This indicates that mechanical alteration via the impact process is not primarily responsible for the observed ejecta compositions; in addition, this example (Fig. 13) indicates that the rock unit varies in thickness.

The observations above suggest that the mafic rocky unit stratigraphically overlies the undifferentiated plains. However, there are areas where plains-like materials that are not part of crater ejecta blankets appear to lie above the rocky unit (Fig. 14). Thus, the stratigraphic relationship between these two units is not clear. If the plains unit is solely indurated material, the data indicate that plains-like material is found both stratigraphically above and below the mafic rocky unit. This would imply a change in conditions to produce the mafic rocky material (such as volcanic activity), followed by a rapid return to pre-rocky unit conditions.

We view this scenario as unlikely, and suggest instead that the undifferentiated plains at least partially consist of mobile sediment. Features indicative of erosion in indurated material are absent in the plains unit. In addition, aeolian bedforms are commonly observed on the low-albedo plains (Section 3.3), further supporting the idea that the plains materials are partially unconsolidated. However, it is clear that not all of the undifferentiated plains materials are unconsolidated. For example, Fig. 15 shows an undifferentiated plains “island” surrounded by mafic rocky material, where

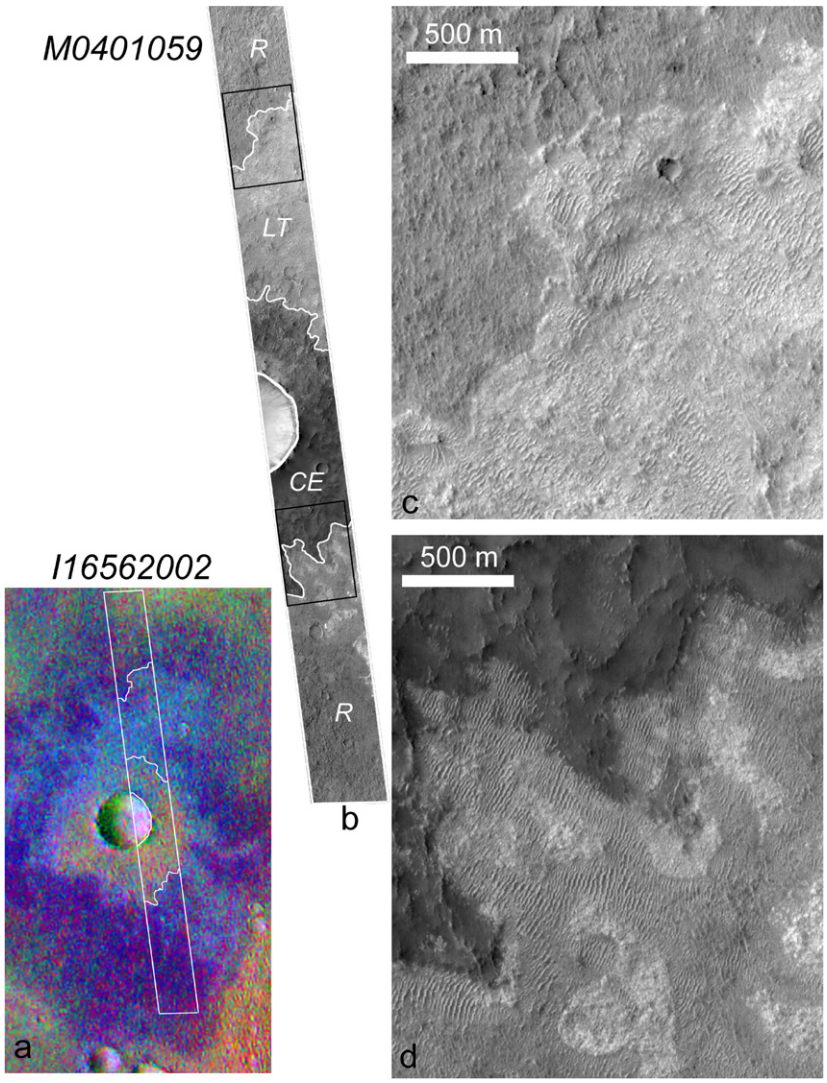

Fig. 10. (a) THEMIS daytime radiance image I16562002, decorrelation stretched using bands 8/7/5 as red–green–blue. Rocky exposures, crater ejecta, and light-toned surfaces are observed in the image. (b) MOC image M04/01059 covers all three of the units in (a). White boxes show locations of closer views in (c) and (d). (For interpretation of the references to color in this figure legend, the reader is referred to the web version of this article.)

Table 3
Characteristics of Mare Serpentis units.

	Rocky unit	Undifferentiated plains	Crater ejecta	Light-toned
Thermal inertia ($J m^{-2} K^{-1} s^{-0.5}$)	>500	120–420	160–270	160–440
Tone/morphology	Variable tone, resistant morphology	Variable tone, variable morphology	Variable tone, variable morphology	Commonly light-toned and superposed by bedforms
THEMIS spectral characteristics	Magenta in DCS 875 (relatively low Band 6–7 emissivity)	Green/yellow in DCS 875 (relatively high Band 6–7 emissivity)	Green/yellow in DCS 875 (relatively high Band 6–7 emissivity)	Light-blue in DCS 875 (similar to undifferentiated plains, but with negative slope imposed on shape)
Composition	Olivine- and pyroxene-rich, less high-silica phases	Olivine- and pyroxene-poor, more high-silica phases	Olivine- and pyroxene-poor, more high-silica phases	N.A.

an ∼ 80 m thick stack of plains material sits isolated on a steep butte. The steep morphology of the butte (∼9°) and sharp margin indicates that it is not a deposit of unconsolidated sediment. Rather, it is either weakly consolidated or there is a thin layer of sediment derived directly from an intact butte of "basement" rock with plains composition (relatively low pyroxene and olivine abundance). Thus we conclude that the upper few centimeters of undifferentiated plains unit consists at least partially (if not entirely) of sediment; still, some areas of the undifferentiated plains may be indurated. The origin of the plains sediment is discussed below.

4.3. Origin of rock and low-TI plains units

The observations presented here demonstrate a major compositional and thermophysical trend present in the study region, with isolated exposures of mafic bedrock and rocky material surrounded by less mafic, lower TI plains. Determining

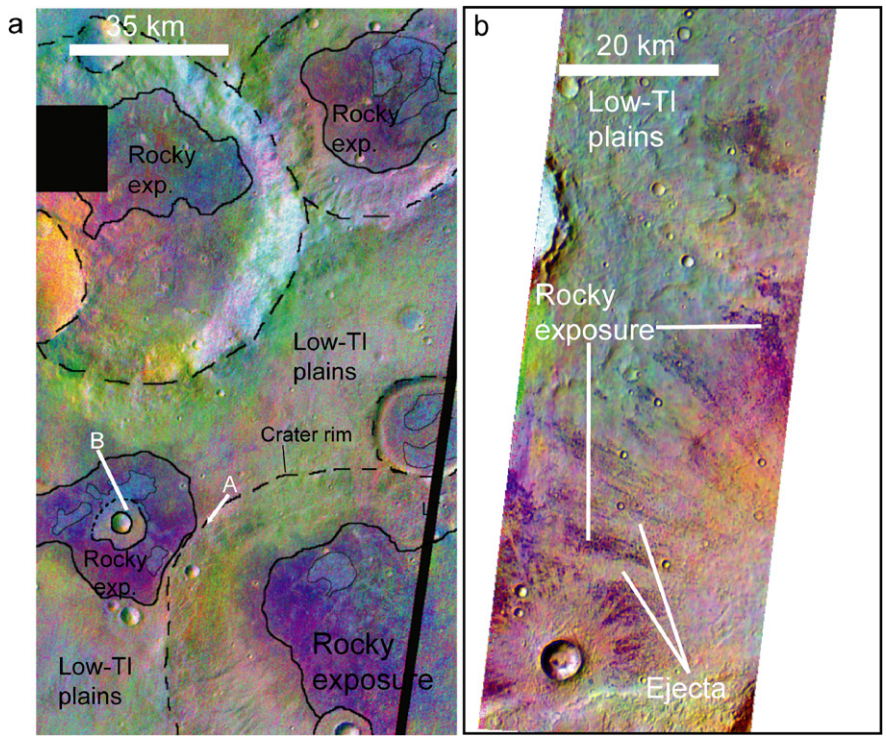

Fig. 11. (a) THEMIS daytime radiance mosaic, decorrelation stretched using bands 8/7/5 as red–green–blue. Regional unit contacts are designated with black lines. "A" points to crater rim that is abutted by a rocky exposure. The proximity of the exposure to the crater rim indicates that the ejecta from the crater underlies the exposure. "B" points to a ~5 km diameter crater that impacted into the rocky exposure. The ejecta blanket from the crater is spectrally identical to the low-TI plains. (b) THEMIS daytime radiance image I01285001, decorrelation stretched using bands 8/7/5 as red–green–blue. The image shows rocky exposures that are partially buried by ejecta from nearby craters. The ejecta is spectrally identical to the low-TI plains. See Fig. 1 for context of these images. (For interpretation of the references to color in this figure legend, the reader is referred to the web version of this article.)

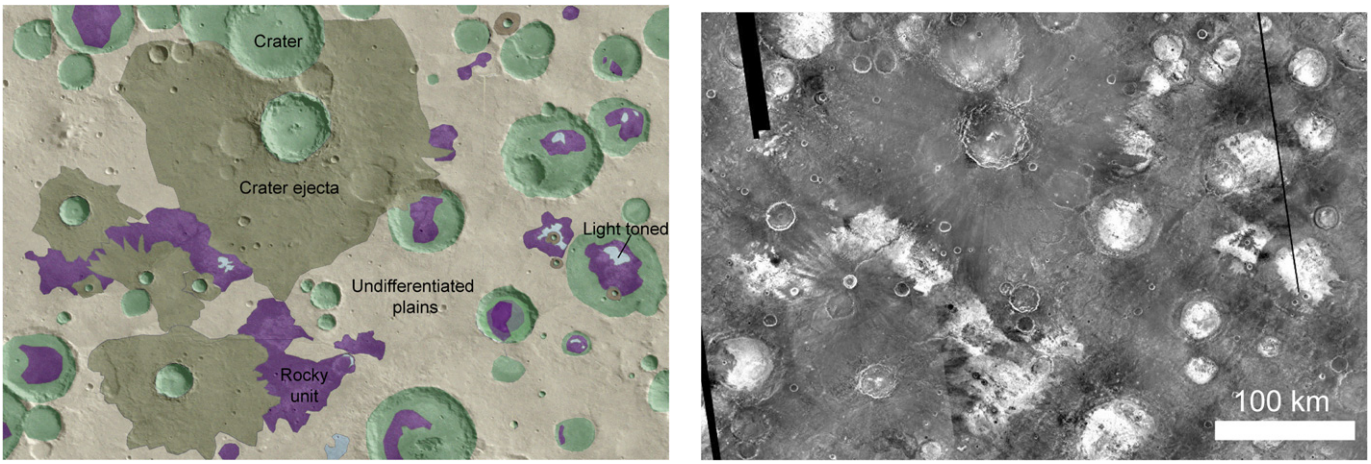

(a) (b)

Fig. 12. (a) Geologic sketch map of a portion of the study region, showing typical unit relationships. (b) THEMIS nighttime infrared radiance mosaic of region in (a), for comparison.

the relationship between these units is crucial to narrowing down potential origins for the mafic rocky materials as well as for interpreting the geologic history of the region. As discussed above, observations of geologic context support the suggestion that the undifferentiated plains unit is at least partially composed of unconsolidated sediment (Section 4.2). Because of the uncertainty in the physical nature of the undifferentiated plains, it is difficult to elucidate the stratigraphic relationship between the rocky and surrounding plains units. Rather, we are limited to putting forth hypotheses for the origin and relationship between these two major units. Two possible scenarios are evaluated (Fig. 16).

4.3.1. Alteration

The first scenario to be considered is that both units originated as a single mafic bedrock unit. In this scenario, the plains materials are derived from the rocky unit, but have been compositionally altered in the process of regolith formation. One potential way to alter the derived materials is through mineral-specific comminution. Hörz et al. (1984) simulated the comminution of rocky surfaces by exposing coarse-grained gabbro fragments (2–32 mm) to hundreds of impacts. They found that the comminuted products became enriched in plagioclase and depleted in pyroxene by 10–15% after only five impacts. For example, the 125–250 μm size fraction consisted of 65–70% plagioclase and 20–25% pyrox-

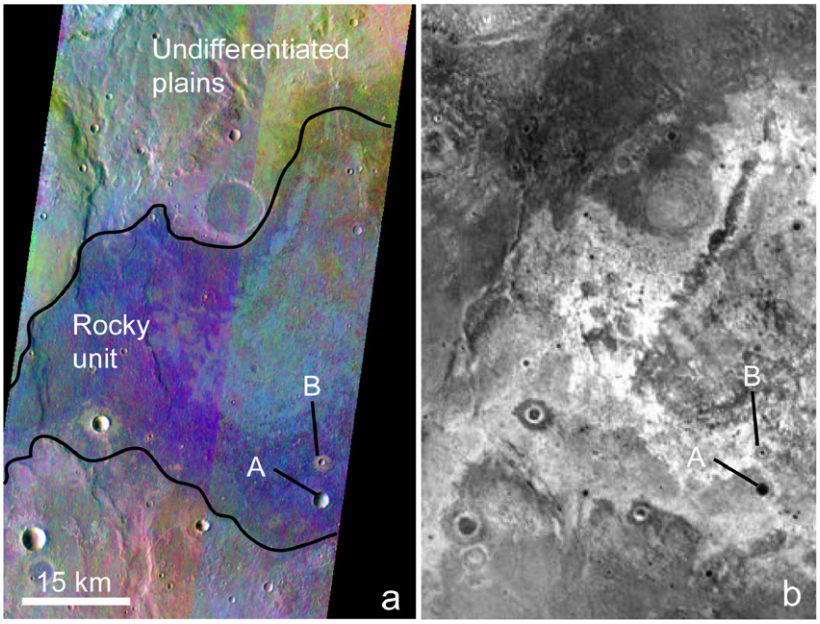

Fig. 13. (a) THEMIS daytime radiance mosaic decorrelation stretched using bands 8/7/5 as red–green–blue. (b) THEMIS nighttime radiance mosaic. "A" points to a ~3 km diameter crater whose impact ejecta is spectrally identical to the rocky unit. "B" points to a nearby crater within the rocky unit, whose ejecta blanket is spectrally identical to undifferentiated plains. The differences in spectral properties of impact materials found within the rocky unit suggest that the unit varies in thickness in this region. See Fig. 1 for context. (For interpretation of the references to color in this figure legend, the reader is referred to the web version of this article.)

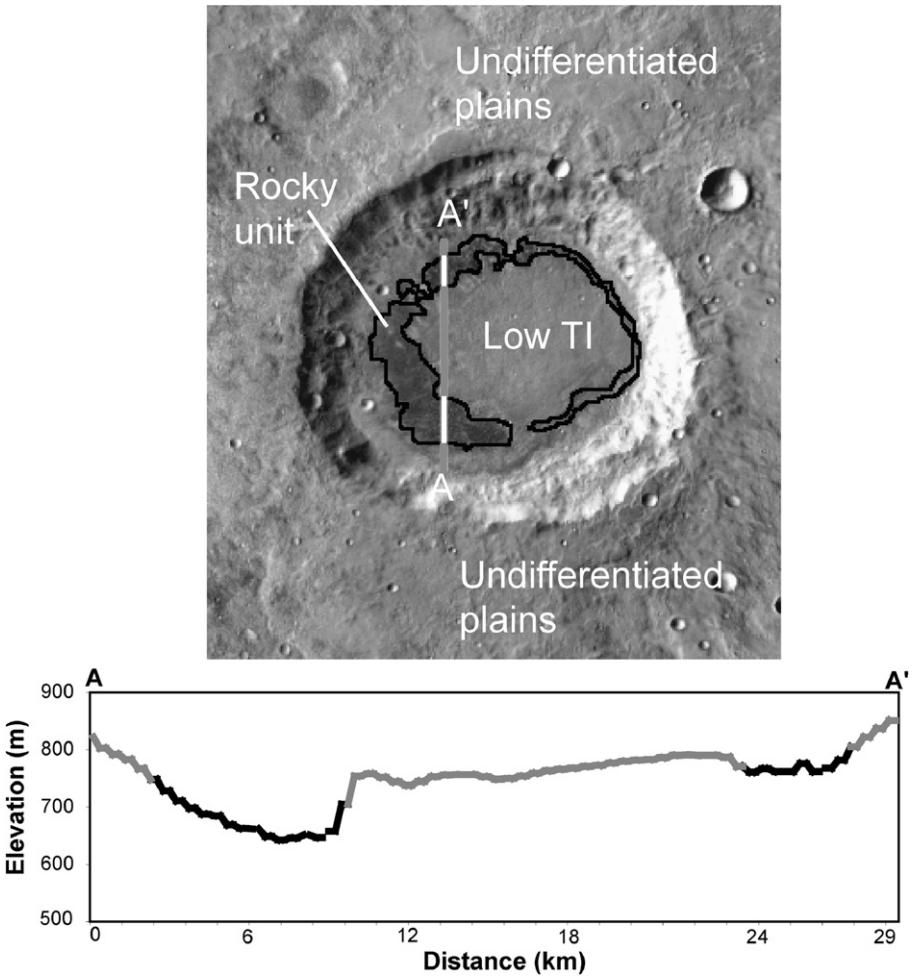

Fig. 14. THEMIS daytime radiance mosaic showing a ~45 km diameter crater with an intracrater rocky exposure. The crater is also host to low TI material (~150–250) which is spectrally identical to the undifferentiated plains. The topographic profile across the crater floor suggests that the low TI material overlies the rocky unit. The low TI material is interpreted here as reworked plains material which has been deposited on top of the intracrater rocky unit. See Fig. 1 for context.

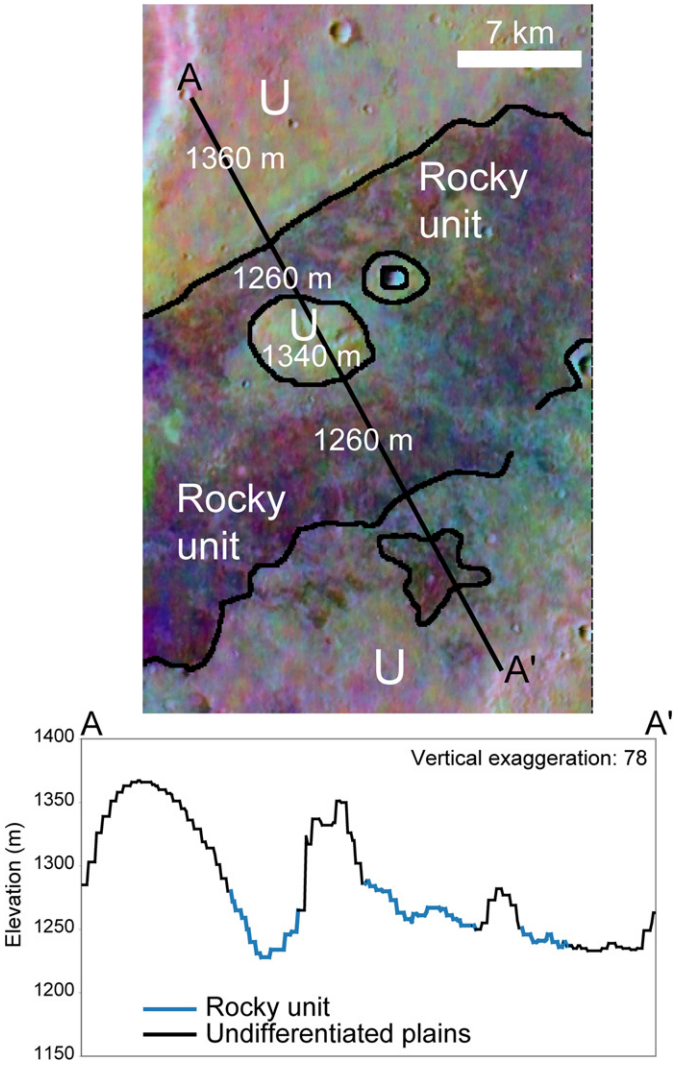

Fig. 15. Portion of THEMIS daytime radiance image I08226002 decorrelation stretched using bands 9/6/4 as red–green–blue. The image shows an isolated butte of plains-like composition, surrounded by rocky material. The sharp margins and steep-sided nature of the butte (~16% grade) suggests that it cannot be comprised entirely of sediment. See Fig. 1 for context. (For interpretation of the references to color in this figure legend, the reader is referred to the web version of this article.)

ene, while the initial target fragments consisted of 54% plagioclase and 33% pyroxene. These mineral-specific differential comminution trends were also found for olivine-bearing gabbros. Pyroxene and olivine are most resistant to break down, while quartz and plagioclase are less resistant (Hörz et al., 1986). Applying this process to units in Mare Serpentis, the laboratory results suggest that the bedrock exposures would become less extensive through impact erosion over time, and the fine component of the regolith would gradually become enriched in plagioclase relative to the remaining rocky material.

A second way to produce pyroxene- and olivine-depleted sediment from pyroxene- and olivine-rich rock is through chemical interaction with acidic water or fog (e.g., Banin et al., 1992). Rock rinds and interiors measured in Gusev crater suggest that the martian weathering environment has been dominated by acidic and water-limited conditions. Tosca et al. (2004) show that olivine is one of the first phases to be dissolved from basalt in acidic solutions. Similarly, McAdam et al. (2008) use dissolution modeling to demonstrate that plagioclase/pyroxene ratios can increase through exposure to fluids with pH < 3. Basalt dissolution experiments at higher temperatures, however, resulted in a *decrease* of plagioclase/pyroxene ratio at low pH (Hurowitz et al., 2005). These studies combined suggest that the dissolution behavior may be dependent on temperature and possibly starting composition. In Mare Serpentis, it is possible that thin films of water on the bedrock dissolved pyroxene and olivine, leaving behind a plagioclase-rich rind. This rind would break down easily into plagioclase-rich sediment (McAdam et al., 2008), leaving behind an unaltered bedrock surface enriched in olivine and pyroxene. Alternatively, sediment could be generated from the rock without alteration. These small particles, with larger surface area than the rocky material, could then be preferentially altered later on through olivine and pyroxene dissolution. Alteration of olivine-rich bedrock to produce olivine-depleted sediment is almost certainly occurring in other locations on Mars, including Gusev Crater (Hurowitz et al., 2006) and Argyre Planitia (Bandfield and Rogers, 2008). In Argyre Planitia, the source of the olivine-depleted sediment (olivine-rich bedrock) is clearly observed, leaving little doubt about the genetic relationship between the two units.

The differences in mineralogical composition between the two major unit types are consistent with general weathering trends suggested for Mars (Fig. 17) (Hurowitz and McLennan, 2007). This observation lends support to the common-origin/alteration hypothesis. However, these compositional differences could just as easily be produced in the absence of an alteration process.

4.3.2. Stratigraphically distinct crustal units

The second hypothesis is that the mafic rocky unit stratigraphically overlies an older, more degraded, plains "basement" unit (Fig. 16). In this scenario, the relatively pyroxene- and olivine-poor plains composition may represent a primary igneous lithology or weathered mafic material. The rocky unit was deposited in isolated exposures on top of the older plains either through volcanism or through sediment transport and deposition. These exposures may have been more extensive in the past. Subsequent aeolian, impact, and/or fluvial activity modified the margins of the rocky unit, and contributed to partial burial of the mafic rock by less mafic material. The plains and rocky units may have originally formed with similar compositions, but with the older plains materials exposed to greater or more prolonged mechanical and/or chemical weathering conditions than the younger rocky unit.

There are two observations that lend support to this hypothesis. First, crater ejecta from craters ~3 km diameter or larger are compositionally identical to the surrounding plains. If the mafic rocky unit overlies a less mafic unit, and is relatively thin, then craters above ~3 km diameter should have little contribution from the rocky unit, as is observed. Second, if the pyroxene-poor nature of the plains is only surficial, as would be implied by the alteration hypothesis, it is expected that fresh craters would expose more mafic material. Small, presumably fresh craters with TI values of ~500 more commonly appear spectrally identical to the plains (Fig. 18).

If the mafic rocky unit does represent a relatively younger unit than the majority of the basement material it overlies, then what is its origin? There are no diagnostic morphologic features that indicate a volcanic or sedimentary origin, however there are a few observations worth noting. First, if the mafic exposures are sandstones, there must be a source of that sand. However, no obvious sources or transport pathways are observed. There is also no apparent control on the depositional locations of the sand. The rocky unit is commonly found in relative topographic lows, but there are several exceptions. In addition, there are numerous relatively low areas where no mafic material is found. The dispersed distribution of the mafic material in isolated locations and variable elevations would be entirely consistent with a volcanic origin, however.

Low ridges 600–700 km in length identified near Huygens Crater (just northeast of Mare Serpentis) have been cited as evi-

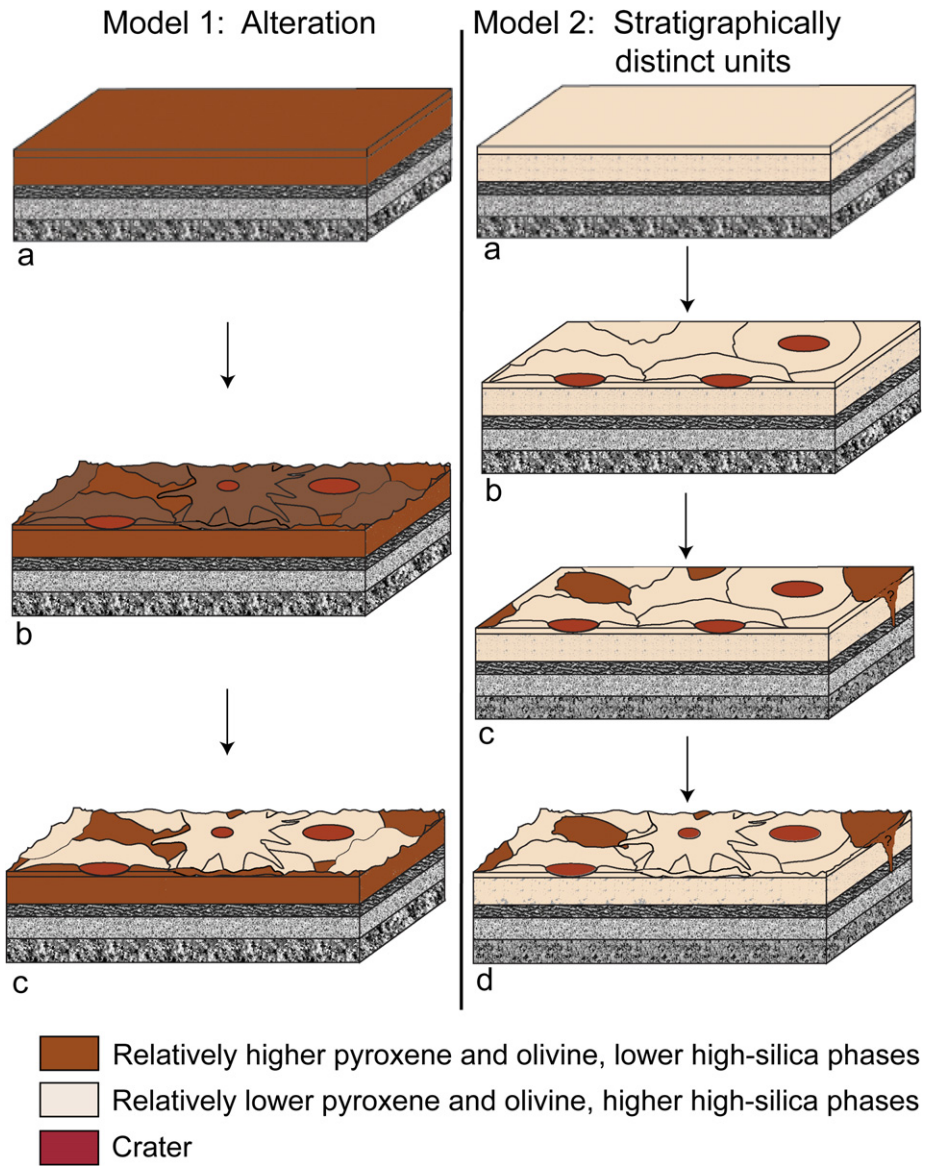

Fig. 16. Two models put forth to explain the present day spatial trends in composition and thermophysical properties. Model 1, alteration: (a) Start with upper crust of rocky unit composition (Table 2, relatively pyroxene and olivine-rich). (b) Reworking of surface material through cratering, aeolian, and fluvial action, and generation of sediment. (c) Preferential dissolution of olivine and pyroxene in finer sediment; isolated exposures of less altered bedrock remain at the surface. Alternatively, sediment could be altered during step (b), through mineral specific comminution (Hörz et al., 1984). Model 2, two stratigraphic units: (a) Start with basement upper crustal unit of undifferentiated plains composition (Table 2, relatively deficient in pyroxene and olivine). The composition may represent a primary igneous lithology or a weathered mafic unit. (b) Degradation of surface material through cratering, aeolian, and fluvial action, and generation of sediment. (c) Local, dispersed deposition of pyroxene- and olivine-rich bedrock material, probably via volcanism. (d) Partial burial of pyroxene- and olivine-rich rocky material by lateral transport of older sediment and impact into degraded plains basement.

dence for basaltic eruptions with very high effusion rates in the late Noachian to early Hesperian time period (Head et al., 2006). It is possible that the isolated mafic rocky exposures are volcanic deposits emplaced as part of this proposed major event.

4.3.3. Summary

In summary, the detailed observations have led us to form two hypotheses for the relationship between these mafic rocky and less mafic sediment units: either they are related through a widespread mechanical and/or chemical alteration process, or they are stratigraphically distinct units representing separate episodes of upper crust formation. Existing observations favor the latter scenario, but it is possible that both processes have contributed to surface development in this area. Either scenario would have important implications for current understanding of crust formation and regolith evolution on ancient Mars. These hypotheses should be testable with collection of decimeter-resolution imagery and decameter-resolution short wavelength infrared spectra.

4.4. Relationship between the Mare Serpentis rocky unit, other martian rocks, and the regolith fine component

The rock exposures described here are similar in composition to sands observed at Meridiani Planum with TES and Mars Exploration Rover data (Rogers and Aharonson, 2008). The source of Meridiani sands are unknown, however it is possible that rock compositions similar to those of the Mare Serpentis rocky unit exist near the Meridiani Planum region or at depth below the Burns formation (a sulfate-rich sedimentary unit in Meridiani Planum) (McLennan et al., 2005). As discussed above, preliminary work suggests that bedrock units with this composition may extend to other highland regions.

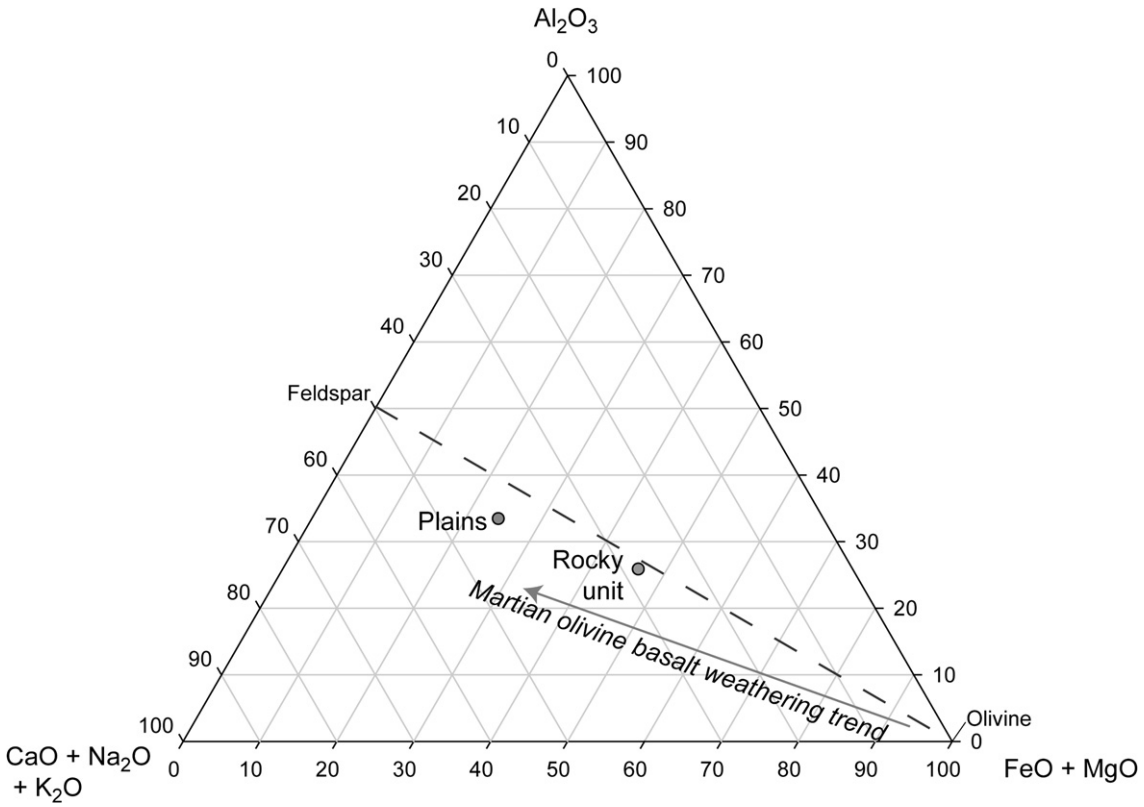

Fig. 17. Arrow represents the general weathering trend proposed for olivine basalts on Mars, based on in situ compositional measurements at Gusev crater and basalt dissolution experiments (Hurowitz and McLennan, 2007). The trend is for a weathering environment dominated by acidic and water limited conditions. The circles represent the average composition of the primary mineral components (feldspar, pyroxene, and olivine) from plains and rocky units in Table 2.

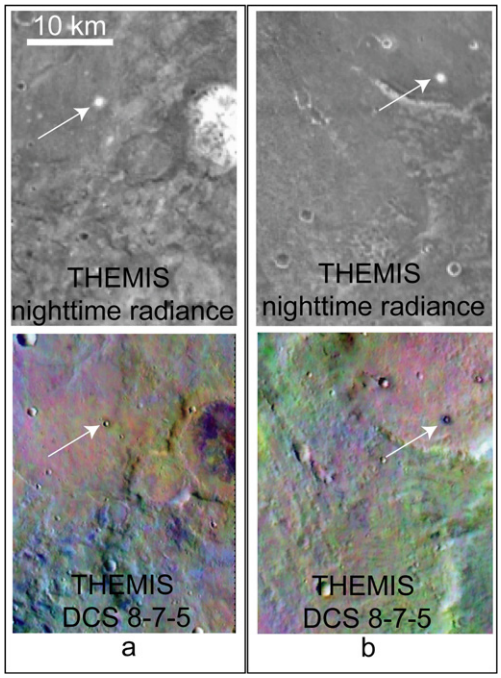

Fig. 18. (a) Typical spectral character of "fresh" crater ejecta found within the undifferentiated plains. THEMIS derived TI of the crater ejecta is ~500. The crater ejecta blanket is spectrally indistinguishable from the surrounding plains. (b) Rare example of fresh crater ejecta that is more spectrally similar to rocky units than the plains. THEMIS derived TI of the crater ejecta is ~500.

Neither the rock nor low-TI plains compositions in Mare Serpentis are reasonably comparable to plains basalts in Gusev Crater. Gusev plains basalts, though exhibiting high abundances of plagioclase and pyroxene, have relatively high olivine contents (~20–30%) (McSween et al., 2006; McSween et al., 2008). The differences in composition are not surprising, given the distance between Gusev Crater and the study region.

An average mineralogic composition for the surface layer in Noachian highland regions was derived from TES data ("Group 3" of Rogers and Christensen, 2007). An unresolved question in that study was whether the derived regional composition represents a mixture of compositionally distinct local-scale units, or a relatively uniform surface composition across the region. The Group 3 composition is not a satisfactory match to either Mare Serpentis bedrock or surrounding plains, but is consistent with a mixture of the two units. This suggests that regional compositions derived with TES data (e.g., Rogers and Christensen, 2007) likely represent a mixture of small-scale geologic units with differing compositions rather than to a region of uniform composition.

The rocky unit composition presented here exhibits a low plagioclase/pyroxene ratio relative to many regions of the low albedo regolith fine component (Rogers and Christensen, 2007), and is more similar to martian meteorite compositions than this fine material. Several recent analyses, including this study, have presented evidence that meteorite-like compositions are exposed at the surface of Mars, and span a variety of surface ages and thermophysical properties (e.g., Hamilton et al., 2003; Christensen et al., 2004; Rogers and Christensen, 2007; Stockstill-Cahill et al., 2008).

5. Conclusions

From the observations presented here, we conclude the following:

1. A major compositional and thermophysical trend is observed in the study region, with isolated exposures of mafic rocky

material surrounded by less mafic, lower thermal inertia plains. Preliminary work outside the study area suggests that this trend extends to other highland regions, but this must be verified with more detailed study. Observations of olivine-depleted sediment eroded from olivine-rich bedrock in Argyre basin gullies (Bandfield and Rogers, 2008) are one established example.

2. Two hypotheses for the relationship between mafic rock and less mafic, low-TI plains units are put forth: either they are related through a widespread mechanical and/or chemical alteration process, or they are stratigraphically distinct units representing separate episodes of upper crust formation. It is possible that both scenarios are applicable to surface development in this area. Existing observations suggest that the second scenario is more likely. In this scenario, plains materials represent degraded, and possibly altered, "basement" rock, whereas the mafic rocky exposures represent later, volumetrically minor additions to the crust and are probably volcanic in origin.
3. Isolated rocky exposures in the Mare Serpentis region exhibit remarkably similar compositions, yet are dispersed over an area of $>10^6$ km^2.
4. Previously derived compositions for the fine component of the regolith (e.g., Rogers and Christensen, 2007) in highland low-albedo regions are similar to a mixture of rock and low-TI plains compositions observed in Mare Serpentis. There are no extreme differences observed between rock exposures and the low TI material (the differences are manifested as variable abundances of plagioclase, pyroxene and olivine, rather than as unique mineral assemblages), suggesting that they are closely linked.

Acknowledgments

We are grateful for THEMIS-derived thermal inertia images provided by Robin Fergason. Sarah Gelman, under sponsorship by the Caltech SURF program, provided assistance in selecting THEMIS images for thermal inertia analysis. Discussions with Scott McLennan were very helpful. Kimberly Seelos and an anonymous reviewer provided helpful and thorough reviews. This work was supported by the NASA Mars Data Analysis Program (grant NNX06AD94G). MOC images were provided by NASA Malin Space Science Systems. THEMIS images are courtesy of NASA/JPL/Arizona State University.

References

Allen, C.C., Gooding, J.L., Jercinovic, M., Keil, K., 1981. Altered basaltic glass—A terrestrial analog to the soil of Mars. Icarus 45, 347–369.

Arvidson, R.E., Poulet, F., Morris, R.V., Bibring, J.P., Bell, J.F., Squyres, S.W., Christensen, P.R., Bellucci, G., Gondet, B., Ehlmann, B.L., Farrand, W.H., Fergason, R.L., Golombek, M., Griffes, J.L., Grotzinger, J., Guinness, E.A., Herkenhoff, K.E., Johnson, J.R., Klingelhöfer, G., Langevin, Y., Ming, D., Seelos, K., Sullivan, R.J., Ward, J.G., Wiseman, S.M., Wolff, M., 2006. Nature and origin of the hematite-bearing plains of Terra Meridiani based on analyses of orbital and Mars Exploration rover data sets. J. Geophys. Res. Planets 111 (E12). E12S08.

Bandfield, J.L., 2002. Global mineral distributions on Mars. J. Geophys. Res. Planets 107 (E6), 5042.

Bandfield, J.L., 2006. Extended surface exposures of granitoid compositions in Syrtis Major, Mars. Geophys. Res. Lett. 33. L06203.

Bandfield, J.L., Rogers, A.D., 2008. Olivine dissolution by acidic fluids in Argyre Planitia, Mars: Evidence for a widespread process? Geology 36, 579–582.

Bandfield, J.L., Smith, M.D., 2003. Multiple emission angle surface–atmosphere separations of Thermal Emission Spectrometer data. Icarus 161 (1), 47–65.

Bandfield, J.L., Christensen, P.R., Smith, M.D., 2000a. Spectral data set factor analysis and end-member recovery: Application to analysis of martian atmospheric particulates. J. Geophys. Res. Planets 105 (E4), 9573–9587.

Bandfield, J.L., Hamilton, V.E., Christensen, P.R., 2000b. A global view of martian surface compositions from MGS-TES. Science 287, 1626–1630.

Bandfield, J.L., Glotch, T.D., Christensen, P.R., 2003. Spectroscopic identification of carbonate minerals in the martian dust. Science 301, 1084–1087.

Bandfield, J.L., Hamilton, V.E., Christensen, P.R., McSween, H.Y., 2004a. Identification of quartzofeldspathic materials on Mars. J. Geophys. Res. Planets 109 (E10), doi:10.1029/2004JE002290. E10009.

Bandfield, J.L., Rogers, D., Smith, M.D., Christensen, P.R., 2004b. Atmospheric correction and surface spectral unit mapping using Thermal Emission Imaging System data. J. Geophys. Res. Planets 110 (E10), doi:10.1029/2004JE002289. E10008.

Banin, A., Clark, B.C., Wanke, H., 1992. Surface chemistry and mineralogy. In: Kieffer, H.H., Jakosky, B., Snyder, C.W., Matthews, M.S. (Eds.), Mars. Univ. of Arizona Press, Tucson, AZ, pp. 594–625.

Bell, J.F., Morris, R.V., Adams, J.B., 1993. Thermally altered Palagonitic Tephra—A spectral and process analog to the soil and dust of Mars. J. Geophys. Res. Planets 98, 3373–3385.

Bibring, J.P., Langevin, Y., Gendrin, A., Gondet, B., Poulet, F., Berthe, M., Soufflot, A., Arvidson, R., Mangold, N., Mustard, J., Drossart, P., Team, O., 2005. Mars surface diversity as revealed by the OMEGA/Mars Express observations. Science 307 (5715), 1576–1581.

Christensen, P.R., 1998. Variations in martian surface composition and cloud occurrence determined from thermal infrared spectroscopy: Analysis of Viking and Mariner 9 data. J. Geophys. Res. Planets 103 (E1), 1733–1746.

Christensen, P.R., Bandfield, J.L., Clark, R.N., Edgett, K.S., Hamilton, V.E., Hoefen, T., Kieffer, H.H., Kuzmin, R.O., Lane, M.D., Malin, M.C., Morris, R.V., Pearl, J.C., Pearson, R., Roush, T.L., Ruff, S.W., Smith, M.D., 2000a. Detection of crystalline hematite mineralization on Mars by the thermal emission spectrometer: Evidence for near-surface water. J. Geophys. Res. Planets 105 (E4), 9623–9642.

Christensen, P.R., Bandfield, J.L., Hamilton, V.E., Howard, D.A., Lane, M.D., Piatek, J.L., Ruff, S.W., Stefanov, W.L., 2000b. A thermal emission spectral library of rock-forming minerals. J. Geophys. Res. Planets 105 (E4), 9735–9739.

Christensen, P.R., Bandfield, J.L., Hamilton, V.E., Ruff, S.W., Kieffer, H.H., Titus, T.N., Malin, M.C., Morris, R.V., Lane, M.D., Clark, R.L., Jakosky, B.M., Mellon, M.T., Pearl, J.C., Conrath, B.J., Smith, M.D., Clancy, R.T., Kuzmin, R.O., Roush, T., Mehall, G.L., Gorelick, N., Bender, K., Murray, K., Dason, S., Greene, E., Silverman, S., Greenfield, M., 2001. Mars global surveyor thermal emission spectrometer experiment: Investigation description and surface science results. J. Geophys. Res. Planets 106 (E10), 23823–23871.

Christensen, P.R., Bandfield, J.L., Bell, J.F., Gorelick, N., Hamilton, V.E., Ivanov, A., Jakosky, B.M., Kieffer, H.H., Lane, M.D., Malin, M.C., McConnochie, T., McEwen, A.S., McSween, H.Y., Mehall, G.L., Moersch, J.E., Nealson, K.H., Rice, J.W., Richardson, M.I., Ruff, S.W., Smith, M.D., Titus, T.N., Wyatt, M.B., 2003. Morphology and composition of the surface of Mars: Mars Odyssey THEMIS results. Science 300 (5628), 2056–2061.

Christensen, P.R., Jakosky, B.M., Kieffer, H.H., Malin, M.C., McSween, H.Y., Nealson, K., Mehall, G.L., Silverman, S.H., Ferry, S., Caplinger, M., Ravine, M., 2004. The Thermal Emission Imaging System (THEMIS) for the Mars 2001 Odyssey Mission. Space Sci. Rev. 110 (1–2), 85–130.

Christensen, P.R., McSween, H.Y., Bandfield, J.L., Ruff, S.W., Rogers, A.D., Hamilton, V.E., Gorelick, N., Wyatt, M.B., Jakosky, B.M., Kieffer, H.H., Malin, M.C., Moersch, J.E., 2005. Evidence for magmatic evolution and diversity on Mars from infrared observations. Nature 436 (7052), 504–509.

Edgett, K.S., Malin, M.C., 2002. Martian sedimentary rock stratigraphy: Outcrops and interbedded craters of northwest Sinus Meridiani and southwest Arabia Terra. Geophys. Res. Lett. 29 (24), doi:10.1029/2002GL016515. 2179.

Edwards, C.S., Bandfield, J.L., Christensen, P.R., Fergason, R.L., 2005. Global distribution of bedrock on Mars using THEMIS high resolution thermal inertia. Eos Trans. AGU (Fall Suppl.) 86 (52). Abstr. P21C-0158.

Farrand, W.H., Bell, J.F., Johnson, J.R., Jolliff, B.L., Knoll, A.H., McLennan, S.M., Squyres, S.W., Calvin, W.M., Grotzinger, J.P., Morris, R.V., Soderblom, J., Thompson, S.D., Watters, W.A., Yen, A.S., 2007. Visible and near-infrared multispectral analysis of rocks at Meridiani Planum, Mars, by the Mars Exploration Rover Opportunity. J. Geophys. Res. Planets 112. E06S02.

Farrand, W.H., Bell, J.F.I., Johnson, J.R., Arvidson, R.E., Crumpler, L., Hurowitz, J.A., Schroder, C., 2008. Rock spectral classes observed by the Spirit Rover's Pancam on the Gusev Crater Plains and in the Columbia Hills. J. Geophys. Res. Planets 113, doi:10.1029/2008JE003237. E12S38.

Fergason, R.L., Christensen, P.R., Kieffer, H.H., 2006. High-resolution thermal inertia derived from the Thermal Emission Imaging System (THEMIS): Thermal model and applications. J. Geophys. Res. Planets 111 (E12). E12004.

Gendrin, A., Mangold, N., Bibring, J.P., Langevin, Y., Gondet, B., Poulet, R., Bonello, G., Quantin, C., Mustard, J., Arvidson, R., LeMouelic, S., 2005. Sulfates in martian layered terrains: The OMEGA/Mars Express view. Science 307 (5715), 1587–1591.

Gillespie, A.R., 1985. Lithologic mapping of silicate rocks using TIMS. In: The TIMS Data User's Workshop, JPL Pub. 86-38, pp. 29–44.

Gillespie, A.R., Kahle, A.B., Walker, R.E., 1986. Color Enhancement of highly correlated images. I. Decorrelation and HSI contrast stretches. Remote Sens. Environ. 20, 209–235.

Glotch, T.D., Rogers, A.D., 2007. Evidence for aqueous deposition of hematite- and sulfate-rich light-toned layered deposits in Aureum and Iani Chaos, Mars. J. Geophys. Res. Planets 112 (E6), doi:10.1029/2006JE002863. E06001.

Glotch, T.D., Morris, R.V., Christensen, P.R., Sharp, T.G., 2004. Effect of precursor mineralogy on the thermal infrared emission spectra of hematite: Application to Martian hematite mineralization. J. Geophys. Res. Planets 109, doi:10.1029/2003JE002224.

Greeley, R., Guest, J.E., 1987. Geologic map of the eastern equatorial region of Mars, US Geol. Surv. Misc. Invest. Ser. Map I-1802-B.
Greeley, R., Spudis, P.D., 1981. Volcanism on Mars. Rev. Geophys. 19 (1), 13–41.
Hamilton, V.E., 2004. Detailed investigation of a globally unique, orthopyroxene-rich deposit of Eos Chasma, Mars. Eos Trans. AGU (Fall Suppl.) 85. Abstr. #P11A-0959.
Hamilton, V.E., Christensen, P.R., 2005. Evidence for extensive, olivine-rich bedrock on Mars. Geology 33 (6), 433–436.
Hamilton, V.E., Christensen, P.R., McSween, H.Y., Bandfield, J.L., 2003. Searching for the source regions of martian meteorites using MGS TES: Integrating martian meteorites into the global distribution of igneous materials on Mars. Meteorit. Planet. Sci. 38 (6), 871–885.
Head, J.W., Wilson, L., Dickson, J., Neukum, G., 2006. The Huygens–Hellas giant dike system on Mars: Impl ications for late noachian–early hesperian volcanic resurfacing and climatic evolution. Geology 34 (4), 285–288.
Hoefen, T.M., Clark, R.N., Bandfield, J.L., Smith, M.D., Pearl, J.C., Christensen, P.R., 2003. Discovery of olivine in the Nili Fossae region of Mars. Science 302 (5645), 627–630.
Hörz, F., Cintala, M.J., See, T.H., Cardenas, F., Thompson, T.D., 1984. Grain-size evolution and fractionation trends in an experimental regolith. J. Geophys. Res. 89, C183–C196.
Hörz, F., Cintala, M.J., Olds, S., See, T.H., Cardenas, F., 1986. Experimental regolith evolution: Differential comminution of plagioclase, pyroxene and olivine. Lunar Planet. Sci., 362–363.
Hurowitz, J.A., McLennan, S.M., 2007. A similar to 3.5 Ga record of water-limited, acidic weathering conditions on Mars. Earth Planet. Sci. Lett. 260 (3–4), 432–443.
Hurowitz, J.A., McLennan, S.M., Lindsley, D.H., Schoonen, M.A.A., 2005. Experimental epithermal alteration of synthetic Los Angeles Meteorite: Implications for the origin of martian soils and identification of hydrothermal sites on Mars. J. Geophys. Res. Planets 110, doi:10.1029/2005JE002391.
Hurowitz, J.A., McLennan, S.M., Tosca, N.J., Arvidson, R.E., Michalski, J.R., Ming, D.W., Schröder, C., Squyres, S.W., 2006. In situ and experimental evidence for acidic weathering of rocks and soils on Mars. J. Geophys. Res. 111, doi:10.1029/2005JE002515. E02S19.
Lyon, R.J.P., 1965. Analysis of rocks by spectral infrared emission (8 to 25 microns). Econ. Geol. 60, 715–736.
Malin, M.C., 1976. Nature and Origin of Intercrater Plains on Mars. In: Studies of the surface morphology of Mars. Ph.D. dissertation, California Institute of Technology.
McAdam, A.C., Zolotov, M.Y., Sharp, T.G., Leshin, L.A., 2008. Preferential low-pH dissolution of pyroxene in plagioclase–pyroxene mixtures: Implications for martian surface materials. Icarus 196 (1), 90–96.
McLennan, S.M., and 31 colleagues, 2005. Provenance and diagenesis of the evaporite-bearing Burns formation, Meridiani Planum, Mars. Earth Planet. Sci. Lett. 240 (1), 95–121.
McSween, H.Y., and 41 colleagues, 2006. Characterization and petrologic interpretation of olivine-rich basalts at Gusev Crater, Mars. J. Geophys. Res. Planets 111, doi:10.1029/2005JE002477. E02S10.
McSween, H.Y., Ruff, S.W., Morris, R.V., Gellert, R., Klingelhöfer, G., Christensen, P.R., McCoy, T.J., Ghosh, A., Moersch, J.E., Cohen, B.A., Rogers, A.D., Schroeder, C., Squyres, S., Crisp, J.A., Yen, A.S., 2008. Mineralogy of volcanic rocks in Gusev crater, Mars: Reconciling Mossbauer, APXS, and Mini-TES spectra. J. Geophys. Res. Planets, doi:10.1029/2007JE002970.
Michalski, J.R., Kraft, M.D., Diedrich, T., Sharp, T.G., Christensen, P.R., 2003. Thermal emission spectroscopy of the silica polymorphs and considerations for remote sensing of Mars. Geophys. Res. Lett. 30, doi:10.1029/2003GL018354.
Michalski, J.R., Kraft, M.D., Sharp, T.G., Williams, L.B., Christensen, P.R., 2005. Mineralogical constraints on the high-silica martian surface component observed by TES. Icarus 174, 161–177.
Michalski, J.R., Kraft, M.D., Sharp, T.G., Williams, L.B., Christensen, P.R., 2006. Emission spectroscopy of clay minerals and evidence for poorly crystalline aluminosilicates on Mars from Thermal Emission Spectrometer data. J. Geophys. Res. Planets 111. E03004.
Morris, R.V., Gooding, J.L., Lauer, H.V., Singer, R.B., 1990. Origins of Mars-like spectral and magnetic-properties of a Hawaiian palagonitic soil. J. Geophys. Res. Solid Earth Planets 95, 14427–14434.
Murchie, S., Arvidson, R., Bedini, P., Beisser, K., Bibring, J.P., Bishop, J., Boldt, J., Cavender, P., Choo, T., Clancy, R.T., Darlington, E.H., Marais, D.D., Espiritu, R., Fort, D., Green, R., Guinness, E., Hayes, J., Hash, C., Heffernan, K., Hemmler, J., Heyler, G., Humm, D., Hutcheson, J., Izenberg, N., Lee, R., Lees, J., Lohr, D., Malaret, E., Martin, T., McGovern, J.A., McGuire, P., Morris, R., Mustard, J., Pelkey, S., Rhodes, E., Robinson, M., Roush, T., Schaefer, E., Seagrave, G., Seelos, F., Silverglate, P., Slavney, S., Smith, M., Shyong, W.J., Strohbehn, K., Taylor, H., Thompson, P., Tossman, B., Wirzburger, M., Wolff, M., 2007. Compact reconnaissance Imaging Spectrometer for Mars (CRISM) on Mars Reconnaissance Orbiter (MRO). J. Geophys. Res. Planets 112. E05S03.
Mustard, J.F., Poulet, F., Gendrin, A., Bibring, J.P., Langevin, Y., Gondet, B., Mangold, N., Bellucci, G., Altieri, F., 2005. Olivine and pyroxene, diversity in the crust of Mars. Science 307 (5715), 1594–1597.
Mustard, J.F., Poulet, F., Head, J.W., Mangold, N., Bibring, J.P., Pelkey, S.M., Fasset, C.I., Langevin, Y., Neukum, G., 2007. Mineralogy of the Nili Fossae region with OMEGA/Mex data. 1. Ancient impact melt in the Isidis basin and implications for the transition from the noachian to hesperian. J. Geophys. Res. Planets 112 (E8). E08S03.
Pelkey, H.Y., and 11 colleagues, 2007. CRISM multispectral summary products: Parameterizing mineral diversity on Mars from reflectance. J. Geophys. Res. Planets 112 (E08). E08S14.
Pieters, C.M., Klima, R.L., Hiroi, T., Dyar, M.D., Lane, M.D., Treiman, A.H., Noble, S.K., Sunshine, J.M., Bishop, J.L., 2008. Martian dunite NWA 2737: Integrated spectroscopic analyses of brown olivine. J. Geophys. Res. Planets 113. E06004.
Poulet, F., Bibring, J.P., Mustard, J.F., Gendrin, A., Mangold, N., Langevin, Y., Arvidson, R.E., Gondet, B., Gomez, C., Team, O., 2005. Phyllosilicates on Mars and implications for early martian climate. Nature 438 (7068), 623–627.
Presley, M.A., Christensen, P.R., 1997. Thermal conductivity measurements of particulate materials. 2. Results. J. Geophys. Res. Planets 102 (E3), 6551–6566.
Putzig, N.E., Mellon, M.T., Kretke, K.A., Arvidson, R.E., 2005. Global thermal inertia and surface properties of Mars from the MGS mapping mission. Icarus 173 (2), 325–341.
Rampe, E.B., Kraft, M.D., Sharp, T.G., Michalski, J.R., 2007. The influence of chemical alteration on thermal infrared spectroscopy and interpretations of igneous mineralogy of Mars. In: Seventh Int. Conf. Mars, Abstr. #3242.
Ramsey, M.S., Christensen, P.R., 1998. Mineral abundance determination: Quantitative deconvolution of thermal emission spectra. J. Geophys. Res. Solid Earth 103 (B1), 577–596.
Rogers, A.D., Christensen, P.R., 2007. Surface mineralogy of martian low-albedo regions from MGS-TES data: Implications for upper crustal evolution and surface alteration. J. Geophys. Res. Planets 112 (E1). E01003.
Rogers, A.D., Aharonson, O., 2008. Mineralogical composition of sands in Meridiani Planum determined from MER data and comparison to orbital measurements. J. Geophys. Res. Planets 113 (E06), doi:10.1029/2007JE002995. E06S14.
Rogers, A.D., Christensen, P.R., Bandfield, J.L., 2005. Compositional heterogeneity of the ancient martian crust: Surface analysis of Ares Vallis bedrock with THEMIS and TES data. J. Geophys. Res. Planets 110, doi:10.1029/2005JE002399. E05010.
Roush, T.L., Blaney, D.L., Singer, R.B., 1993. The surface composition of Mars as inferred from spectroscopic observations. In: Pieters, C.M., Englert, P.A.J. (Eds.), Remote Geochemical Analysis: Elemental and Mineralogical Composition. Cambridge University Press, Cambridge, UK.
Ruff, S.W., 2004. Spectral evidence for zeolite in the dust on Mars. Icarus 168, 131–143.
Ruff, S.W., Christensen, P.R., 2002. Bright and dark regions on Mars: Particle size and mineralogical characteristics based on Thermal Emission Spectrometer data. J. Geophys. Res. Planets 107, doi:10.1029/2001JE001580, 5127.
Ruff, S.W., Christensen, P.R., Blaney, D.L., Farrand, W.H., Johnson, J.R., Michalski, J.R., Moersch, J.E., Wright, S.P., Squyres, S., 2006. The rocks of Gusev Crater as viewed by the Mini-TES instrument. J. Geophys. Res. Planets 111. E12S18.
Singer, R.B., McCord, T.B., Clark, R.N., Adams, J.B., Huguenin, R.L., 1979. Mars surface-composition from reflectance spectroscopy—Summary. J. Geophys. Res. 84, 8415–8426.
Smith, M.D., Bandfield, J.L., Christensen, P.R., 2000. Separation of atmospheric and surface spectral features in Mars Global Surveyor Thermal Emission Spectrometer (TES) spectra. J. Geophys. Res. Planets 105 (E4), 9589–9607.
Smith, D.E., and 23 colleagues, 2001. Mars Orbiter Laser Altimeter: Experiment summary after the first year of global mapping of Mars. J. Geophys. Res. Planets 106 (E10), 23689–23722.
Soderblom, L.A., 1992. The composition and mineralogy of the martian surface from spectroscopic observations: 0.3 microns to 50 microns. In: Kieffer, H.H., Jakosky, B., Snyder, C.W., Matthews, M.S. (Eds.), Mars. Univ. of Arizona Press, Tucson, pp. 557–593.
Stockstill-Cahill, K.R., Anderson, F.S., Hamilton, V.E., 2008. A study of low-albedo deposits within Amazonis Planitia craters: Evidence for locally derived ultramafic to mafic materials. J. Geophys. Res. Planets 113. E07008.
Tanaka, K.L., Isbell, N.K., Scott, D.H., Greeley, R., Guest, J.E., 1988. The resurfacing history of Mars: A synthesis of digitized, Viking-based geology. Proc. Lunar Sci. Conf. 18, 665–678.
Tosca, N.J., McLennan, S.M., Lindsley, D.H., Schoonen, M.A.A., 2004. Acid–sulfate weathering of synthetic martian basalt: The acid fog model revisited. J. Geophys. Res. Planets 109 (E5). E05003.
Wyatt, M.B., Hamilton, V.E., McSween, H.Y., Christensen, P.R., Taylor, L.A., 2001. Analysis of terrestrial and martian volcanic compositions using thermal emission spectroscopy. 1. Determination of mineralogy, chemistry, and classification strategies. J. Geophys. Res. Planets 106, 14711–14732.